Insight into the RNA Exosome Complex Through Modeling Pontocerebellar Hypoplasia Type 1b Disease Mutations in Yeast

Milo B. Fasken,*,[1] Jillian S. Losh,[†,‡,1] Sara W. Leung,* Sergine Brutus,*,[§] Brittany Avin,*, Jillian C. Vaught,[†] Jennifer Potter-Birriel,*,[††] Taylor Craig,* Graeme L. Conn,[‡‡] Katherine Mills-Lujan,* Anita H. Corbett,*,[2] and Ambro van Hoof[†,‡,2]**

*Department of Biology, [‡‡]Department of Biochemistry, [§]Emory Initiative for Maximizing Student Diversity, **Emory Summer Undergraduate Research Experience Program, and [††]Emory Postbaccalaureate Training Program, Emory University, Atlanta, Georgia 30322, [†]Department of Microbiology and Molecular Genetics, University of Texas Health Science Center-Houston, and [‡]The University of Texas Graduate School of Biomedical Sciences, Houston, Texas 77030

ABSTRACT Pontocerebellar hypoplasia type 1b (PCH1b) is an autosomal recessive disorder that causes cerebellar hypoplasia and spinal motor neuron degeneration, leading to mortality in early childhood. PCH1b is caused by mutations in the RNA exosome subunit gene, *EXOSC3*. The RNA exosome is an evolutionarily conserved complex, consisting of nine different core subunits, and one or two 3′-5′ exoribonuclease subunits, that mediates several RNA degradation and processing steps. The goal of this study is to assess the functional consequences of the amino acid substitutions that have been identified in EXOSC3 in PCH1b patients. To analyze these EXOSC3 substitutions, we generated the corresponding amino acid substitutions in the *Saccharomyces cerevisiae* ortholog of EXOSC3, Rrp40. We find that the rrp40 variants corresponding to EXOSC3-G31A and -D132A do not affect yeast function when expressed as the sole copy of the essential Rrp40 protein. In contrast, the rrp40-W195R variant, corresponding to EXOSC3-W238R in PCH1b patients, impacts cell growth and RNA exosome function when expressed as the sole copy of Rrp40. The rrp40-W195R protein is unstable, and does not associate efficiently with the RNA exosome in cells that also express wild-type Rrp40. Consistent with these findings in yeast, the levels of mouse EXOSC3 variants are reduced compared to wild-type EXOSC3 in a neuronal cell line. These data suggest that cells possess a mechanism for optimal assembly of functional RNA exosome complex that can discriminate between wild-type and variant exosome subunits. Budding yeast can therefore serve as a useful tool to understand the molecular defects in the RNA exosome caused by PCH1b-associated amino acid substitutions in EXOSC3, and potentially extending to disease-associated substitutions in other exosome subunits.

KEYWORDS pontocerebellar hypoplasia type 1b; RNA exosome; EXOSC3; Rrp40; EXOSC2; RNA processing/degradation

THE RNA exosome is an evolutionarily conserved ribonuclease complex that is responsible for several essential RNA processing and degradation steps (Mitchell *et al.* 1997; Allmang *et al.* 1999; Schneider and Tollervey 2013). Major exosome substrates include mRNA, rRNA, and small RNAs. In addition to degrading aberrant and unneeded transcripts, the RNA exosome also trims precursor RNAs, including 5.8S rRNA (Mitchell *et al.* 1996). The RNA exosome thus plays critical roles in both RNA degradation and maturation.

The subunits of the RNA exosome complex are evolutionarily conserved and many were first identified in *Saccharomyces cerevisiae* in a screen for **r**ibosomal **R**NA **p**rocessing (*rrp*) mutants (Mitchell *et al.* 1996, 1997; Allmang *et al.* 1999). *S. cerevisiae* Rrp subunits correspond to human EXOSC subunits. The functions of the RNA exosome have been extensively characterized in budding yeast (Sloan *et al.* 2012), and many are conserved in humans (Schilders *et al.* 2005; Staals *et al.* 2010; Lubas *et al.* 2011, 2015). Within

doi: 10.1534/genetics.116.195917
Manuscript received September 13, 2016; accepted for publication October 19, 2016; published Early Online October 24, 2016.
Supplemental material is available online at www.genetics.org/lookup/suppl/doi:10.1534/genetics.116.195917/-/DC1.
[1]These authors contributed equally to this work.
[2]Corresponding authors: Department of Biology, Emory University, 1021RRC, 1510 Clifton Rd. NE, Atlanta, GA 30322. E-mail: acorbe2@emory.edu; and Department of Microbiology and Molecular Genetics, University of Texas Health Science Center-Houston, 6431 Fannin St., MSB 1.212, Houston, TX 77030. E-mail: Ambro.van.hoof@uth.tmc.edu

the RNA exosome, six subunits comprise a core ring, and three putative RNA-binding subunits, including EXOSC3, form a cap that interacts with the core ring on one side of the complex (Figure 1A). The catalytic DIS3 subunit, which possesses both endo and exoribonuclease activities (Dziembowski *et al.* 2007; Lebreton *et al.* 2008; Schaeffer *et al.* 2009), associates with the opposite side of the core ring from the cap (Figure 1A) (Malet *et al.* 2010; Staals *et al.* 2010; Tomecki *et al.* 2010; Makino *et al.* 2013). RNA substrates can be threaded through the central channel of the core ring from the EXOSC3/cap side (Liu *et al.* 2006; Bonneau *et al.* 2009; Malet *et al.* 2010; Makino *et al.* 2013). Additional RNA entry points have also been identified (Liu *et al.* 2014; Wasmuth *et al.* 2014; Han and van Hoof 2016) that could provide insight into how the RNA exosome balances precise processing and complete degradation of RNA.

The RNA exosome is present in both the nucleus and the cytoplasm. Nuclear and cytoplasmic RNA exosomes also require specific exosome cofactors (Butler and Mitchell 2010; Schaeffer *et al.* 2010), which help to guide the degradation and/or processing of specific RNAs. In particular, the cytoplasmic cofactor, the SKI complex, is required for all known cytoplasmic functions of the RNA exosome, but not for its nuclear functions (Jacobs Anderson and Parker 1998; van Hoof *et al.* 2000). Importantly, exosome cofactors characterized in budding yeast (Jacobs Anderson and Parker 1998; Allmang *et al.* 1999; Brown *et al.* 2000; van Hoof *et al.* 2000; LaCava *et al.* 2005; Vasiljeva and Buratowski 2006), are conserved in Metazoa, and possess conserved functions in humans (Schilders *et al.* 2007; Shcherbik *et al.* 2010; Lubas *et al.* 2011; Kowalinski *et al.* 2016).

Defects in the RNA exosome, and exosome cofactors, have been implicated in several genetic diseases. Mutations in SKI complex genes have been linked to tricho-hepato-enteric (THE) syndrome, which causes intestinal failure (Hartley *et al.* 2010; Fabre *et al.* 2012, 2013). In addition, mutations in the *DIS3* catalytic subunit gene have been implicated in multiple myeloma (Chapman *et al.* 2011; Tomecki *et al.* 2013; Robinson *et al.* 2015). Recently, mutations in genes encoding structural exosome subunits have been linked to neurological diseases (Wan *et al.* 2012; Boczonadi *et al.* 2014; Di Donato *et al.* 2016). Mutations in the gene encoding the RNA exosome cap subunit, EXOSC3 (Figure 1, B and C), have been linked to pontocerebellar hypoplasia type 1b (PCH1b) (Wan *et al.* 2012). PCH1b does not appear to share common traits with THE syndrome or multiple myeloma. Instead, PCH1b patients exhibit significant atrophy of the pons and cerebellum, Purkinje cell abnormalities, and degeneration of spinal motor neurons (Wan *et al.* 2012). PCH1b patients also show microcephaly, muscle atrophy, and growth and developmental retardation (Rudnik-Schoneborn *et al.* 2013). Most PCH1b patients do not live past childhood. Elucidation of the molecular mechanisms that underlie PCH1b is therefore of critical importance for the development of new treatments.

Pontocerebellar hypoplasia (PCH) is a group of recessive, autosomal disorders caused by mutations in several genes. Like PCH1b, PCH1c is caused by mutations in a gene encoding an RNA exosome core subunit, EXOSC8 (Boczonadi *et al.* 2014) (Figure 1A). However, most PCH subtypes are caused by mutations in genes encoding tRNA splicing endonuclease subunits that function in tRNA processing (PCH2a, 2b, 2c, 4, 5, and 10) (Budde *et al.* 2008; Namavar *et al.* 2011; Hanada *et al.* 2013; Schaffer *et al.* 2014), a selenocysteinyl tRNA charging enzyme (PCH2d) (Agamy *et al.* 2010) or a mitochondrial arginyl-tRNA synthetase (PCH6) (Edvardson *et al.* 2007). A few PCH subtypes are caused by mutations that have no apparent link to the RNA exosome or tRNA, such as in genes encoding vaccinia-related kinase (PCH1a) (Renbaum *et al.* 2009), chromatin modifying protein 1A (PCH8) (Akizu *et al.* 2013), and adenosine monophosphate deaminase 2 (PCH9) (Mochida *et al.* 2012). Understanding how these disparate gene mutations cause PCH diseases with common traits requires study of the functional defects that lead to disease.

Currently, it is unclear how the amino acid substitutions in EXOSC3 contribute to PCH1b disease, but it is unlikely that PCH1b is caused by complete inactivation of the RNA exosome as this complex is essential even in budding yeast (Mitchell *et al.* 1997). EXOSC3 amino acid substitutions may cause PCH1b by several potential mechanisms. First, EXOSC3 changes could affect a subset of RNA exosome functions. In yeast, mutations in another RNA exosome cap subunit gene, *CSL4*, disrupt some, but not other, functions of the RNA exosome (van Hoof *et al.* 2000). Second, EXOSC3 amino acid changes could affect RNA exosome-mediated degradation of tRNAs. The yeast RNA exosome degrades tRNAs (Wichtowska *et al.* 2013) and misprocessed precursors of initiator tRNAs (Kadaba *et al.* 2004). Third, EXOSC3 changes could reduce total RNA exosome activity. Finally, EXOSC3 changes could impair functions of EXOSC3 that are independent of the RNA exosome. This last mechanism seems less likely, as mutations in another exosome subunit gene, *EXOSC8*, cause PCH1c disease (Boczonadi *et al.* 2014).

To begin to address the molecular defects that underlie PCH1b disease, we have generated and analyzed amino acid substitutions in the budding yeast ortholog of EXOSC3, Rrp40, corresponding to substitutions in PCH1b patients. Unlike most rrp40 variants analyzed, which do not exhibit any discernable phenotypes in yeast, the rrp40-W195R variant, corresponding to EXOSC3-W238R in PCH1b, affects cell growth and RNA exosome function as the sole cellular copy. Moreover, the rrp40-W195R protein is unstable and does not associate efficiently with the RNA exosome in the presence of wild-type Rrp40. Mouse EXOSC3 variant levels are also reduced relative to wild-type EXOSC3 in a neuronal cell line. These results suggest a model for RNA exosome assembly that involves discrimination between wild-type and variant exosome subunits.

Materials and Methods

Saccharomyces cerevisiae strains, plasmids, and chemicals

All DNA manipulations were performed according to standard methods (Sambrook *et al.* 1989), and all media were prepared by standard procedures (Adams *et al.* 1997). All

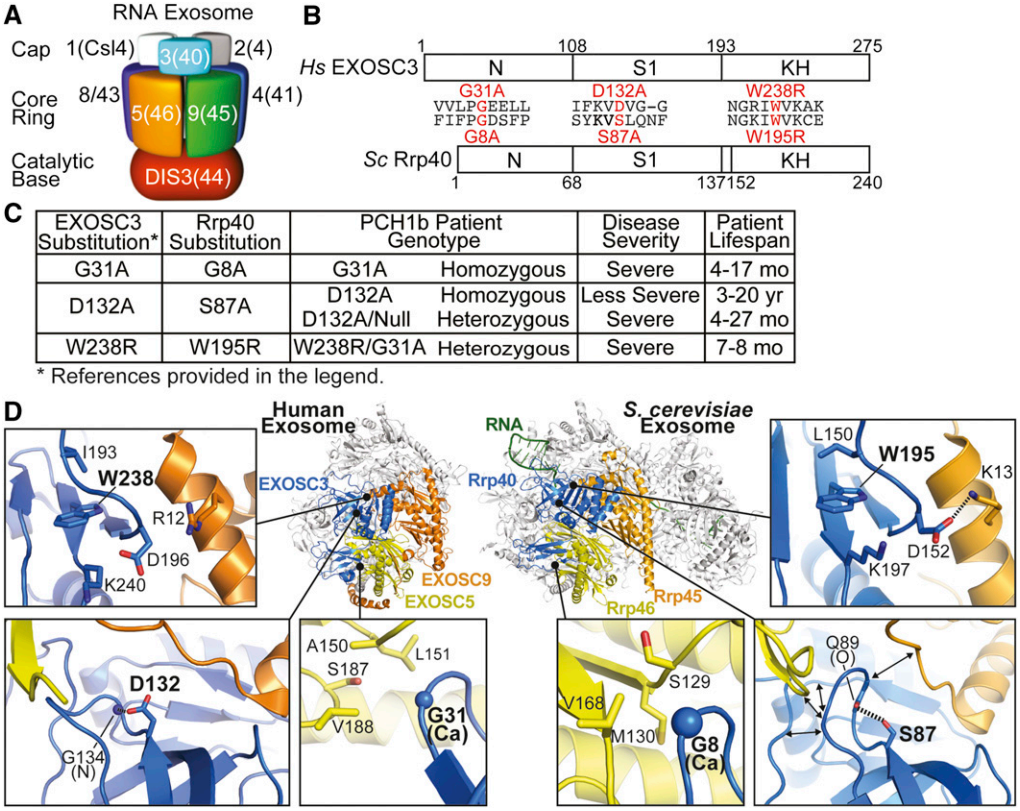

EXOSC3 Substitution*	Rrp40 Substitution	PCH1b Patient Genotype		Disease Severity	Patient Lifespan
G31A	G8A	G31A	Homozygous	Severe	4-17 mo
D132A	S87A	D132A	Homozygous	Less Severe	3-20 yr
		D132A/Null	Heterozygous	Severe	4-27 mo
W238R	W195R	W238R/G31A	Heterozygous	Severe	7-8 mo

* References provided in the legend.

Figure 1 Overview of PCH1b-associated amino acid substitutions in the human EXOSC3 subunit of the RNA exosome, and the corresponding substitutions in the budding yeast ortholog, Rrp40, examined in this study. (A) The RNA exosome is an evolutionarily conserved ribonuclease complex composed of 10 different subunits—three cap subunits: EXOSC1/Csl4 (Human/*S. cerevisiae*); EXOSC2/Rrp4; EXOSC3/Rrp40, six core subunits: EXOSC4/Rrp41; EXOSC5/Rrp46; EXOSC6/Mtr3; EXOSC7/Rrp42; EXOSC8/Rrp43; EXOSC9/Rrp45, and a catalytic base subunit: DIS3/Rrp44. Mutations in the *EXOSC3* gene encoding a cap subunit [light blue, labeled with 3(40)] cause PCH1b (Wan *et al.* 2012), mutations in the *EXOSC8* gene, encoding a core subunit [purple, labeled with 8(43)] cause PCH1c (Boczonadi *et al.* 2014), and mutations in the *EXOSC2* gene, encoding a cap subunit [gray, labeled with 2(4)] cause a novel syndrome (Di Donato *et al.* 2016). (B) EXOSC3 and its budding yeast ortholog, Rrp40, contain three different domains: an N-terminal domain, a central S1 putative RNA binding domain, and a C-terminal putative RNA binding KH (K homology) domain. The position and flanking sequence of the major amino acid substitutions in PCH1b-associated human EXOSC3, and the substitutions generated in the *S. cerevisiae* ortholog of EXOSC3, Rrp40 (shown in red) are indicated. (C) Summary of the major amino acid substitutions identified in EXOSC3 in PCH1b patients (Wan *et al.* 2012) with corresponding substitutions in budding yeast Rrp40 generated in this study. Patient genotypes (Homozygous/Heterozygous) are reported, and disease severity and patient lifespans for each substitution (Wan *et al.* 2012; Schwabova *et al.* 2013; Eggens *et al.* 2014) are also presented to provide some context for the functional consequences of the different amino acid substitutions. (D) PCH1b-associated substitutions occur in EXOSC3 residues located near RNA exosome subunit interfaces. Structural models of the human RNA exosome (left) [PDB#2NN6 (Liu *et al.* 2006)] and *S. cerevisiae* RNA exosome (right) [PDB#4IFD; (Makino *et al.* 2013)] are depicted. The nine subunit human RNA exosome structure highlights the EXOSC3 (blue), EXOSC5 (yellow), and EXOSC9 (yellow) subunits. Zoomed-in views of three subunit interface regions show the locations of PCH1b-associated EXOSC3 substituted residues (G31, D132, and W238 residues in large, bold font). The *S. cerevisiae* RNA exosome structure highlights the orthologous Rrp40 (blue), Rrp46 (yellow), and Rrp45 (orange) subunits. Zoomed-in views show the locations of the evolutionarily conserved residues (G8, S87, and W195). *S. cerevisiae* Rrp40 G8 (EXOSC3 G31) is located in a hydrophobic pocket at an interface with Rrp46 (EXOSC5). Rrp40 S87 (EXOSC3 D132) and the backbone of Q89 are positioned to form a hydrogen bond that may organize the loop between strands β3 and β4, which is at the interface with both Rrp46 (EXOSC5) and Rrp45 (EXOSC9). Rrp40 W195 (EXOSC3 W238) sits in a large pocket, and could be important for positioning the loop of Rrp40 that forms an interface with Rrp45 (EXOSC5).

chemicals were obtained from Sigma-Aldrich (St. Louis, MO), United States Biological (Swampscott, MA), or Fisher Scientific (Pittsburgh, PA), unless otherwise noted. All *S. cerevisiae* strains and plasmids used in this study are listed in Supplemental Material, Table S1. The *rrp40Δ* strain yAV1107 and *rrp4Δ* strain yAV1104 were previously described (Schaeffer *et al.* 2009), as was the *ski7Δ* strain yAV571 (van Hoof *et al.* 2000). The *RRP40-TAP* strain was obtained from GE Dharmacon. The wild-type strain MHY501, and *doa3-1* strain MHY3646, were previously described (Chen and Hochstrasser 1996; Li *et al.* 2007).

The *LEU2 CEN6 RRP40-Myc* (pAC3161) plasmid was constructed by PCR amplification of the *RRP40* promoter, 5′-UTR, and ORF from *RRP40* genomic DNA plasmid (pAC3016), cloning into pRS425 plasmid (Sikorski and Hieter 1989) containing C-terminal *2xMyc* tag and *ADH1* terminator, and PCR amplification and cloning of *RRP40-2xMyc-ADH1* into pRS315. The *LEU2 CEN6 rrp40-G8A-Myc* (pAC3162), *rrp40-S87A-Myc* (pAC3257), *rrp40-W195A-Myc* (pAC3163), *rrp40-W195R-Myc* (pAC3259), and *rrp40-W195F-Myc* (pAC3286) mutant plasmids were generated with *rrp40* oligonucleotides encoding amino acid substitutions, *RRP40-Myc* (pAC3161) plasmid template, and QuikChange Site-Directed Mutagenesis Kit (Stratagene). The *LEU2 CEN6 RRP4* (pAV991) plasmid was constructed by PCR amplification of the *RRP4* from *S. cerevisiae* genomic DNA, and cloning into pRS415 plasmid (Sikorski and Hieter 1989). The *LEU2 CEN6 rrp4-G8A* (pAV1181) and *rrp4-G226D* (pAV1183) mutant plasmids were generated with *rrp4* oligonucleotides encoding amino acid substitutions, *RRP4* (pAV991) plasmid template, and QuikChange Site-Directed Mutagenesis Kit (Stratagene). The pAV188 *his3-nonstop* reporter plasmid was previously described (van Hoof *et al.* 2002).

The *LEU2 RRP40-Myc* and *rrp40-Myc* mutant plasmids were transformed into the *rrp40Δ* strain yAV1107, selected on Ura$^-$ Leu$^-$ plates, and grown on 5-FOA Leu$^-$ plates to select for *rrp40Δ* cells that lack the *URA3 RRP40* plasmid, and contain only the *LEU2 RRP40-Myc* or *rrp40-Myc* plasmid. The *LEU2 RRP40-Myc* and *rrp40-Myc* plasmids were transformed into *RRP40-TAP*, wild-type MHY501, and *doa3-1* MHY3646 strains, and selected on Leu$^-$ plates. The *LEU2 RRP4* and *rrp4* mutant plasmids were transformed into the *rrp4Δ* strain yAV1104, selected on Ura$^-$ Leu$^-$ plates, and grown on 5-FOA Leu$^-$ plates to select for *rrp4Δ* cells that lack the *URA3 RRP4* plasmid, and contain only the *LEU2 RRP4* or *rrp4* plasmid (File S1).

The *Myc-Exosc3* (pAC3417) plasmid was constructed by PCR amplification of murine *Exosc3* ORF (GenBank accession number NM_025513.3) using oligonucleotides (the 5′-primer encoding an N-terminal 2xMyc tag), and mouse cDNA from N2a cells, and cloning into pIGneo (Addgene) plasmid. The *Myc-Exosc3^{G31A}* (pAC3418) and *Myc-Exosc3^{W237R}* (pAC3420) mutant plasmids were generated with *Exosc3* oligonucleotides encoding amino acid substitutions, Myc-*Exosc3* (pAC3417) plasmid template, and QuikChange Site-Directed Mutagenesis Kit (Stratagene). All constructs were sequenced to ensure the presence of each desired mutation, and the absence of any additional mutations.

Saccharomyces cerevisiae growth assays

To test the *in vivo* function of *rrp40* mutants, *rrp40Δ* cells containing *RRP40-Myc* or *rrp40-Myc* mutant plasmid were serially diluted, spotted, and grown on solid medium plates, or grown in liquid medium and measured by recording optical density over time in a microplate reader. The *in vivo* function of *rrp4* mutants was tested in similar growth assays, using *rrp4Δ* cells containing *RRP4* or *rrp4* mutant plasmid. For growth on solid media, *rrp40Δ* (yAV1107) cells containing only *RRP40-Myc* (pAC3161), *rrp40-G8A-Myc* (pAC3162), *rrp40-S87A-Myc* (pAC3257), *rrp40-W195R-Myc* (pAC3259), *rrp40-W195A-Myc* (pAC3163) or *rrp40-W195F-Myc* (pAC3286), or *rrp4Δ* (yAV1104) cells containing only *RRP4* (pAV991), *rrp4-G58V* (pAV1181) or *rrp4-G226D* (pAV1183) plasmid were grown overnight at 30° to saturation in Leu$^-$ minimal medium. Cell concentrations were normalized to OD_{600} = 1, serially diluted in 10-fold dilutions, spotted on Leu$^-$ minimal media plates, or Leu$^-$ minimal media plates containing 25 μM 5-fluorouracil (5-FU), and grown at 25, 30, and 37°. Plates were imaged after 1 and 2 days of growth. In the plasmid shuffle assay, *rrp40Δ* (yAV1107) cells containing *RRP40 URA3* maintenance plasmid and vector (pRS315), *RRP40-Myc* (pAC3161) or *rrp40-Myc* (pAC3161-3163, pAC3257, pAC3259, and pAC3286) were grown overnight at 30° to saturation in Ura$^-$ Leu$^-$ minimal medium. Cell concentrations were normalized and serially diluted, as before, and spotted on Ura$^-$ Leu$^-$ minimal medium plates, or Leu$^-$ minimal medium plates containing 5-fluoroorotic acid (5-FOA), and grown at 25, 30, and 37°. For growth in liquid media, *rrp40Δ* cells (yAV1107) containing only *RRP40-Myc* or *rrp40-Myc* mutant plasmid or rrp4 (yAV1104) containing only *RRP4* or *rrp4* mutant plasmid were grown overnight at 30° to saturation in Leu$^-$ minimal medium, diluted to an OD_{600} = 0.01 in Leu$^-$ minimal media in a 24-well plate, and growth at 37° for *RRP40/rrp40* cells, or 30° for *RRP4/rrp4* cells, was monitored and recorded at OD_{600} in a BioTek SynergyMx microplate reader with Gen5 v2.04 software over 24 hr. Technical triplicates of each strain were measured, and the average of these triplicates was calculated and graphed.

His3-nonstop growth assay

The His3-nonstop growth assay was performed as previously described (Schaeffer *et al.* 2008). *rrp40Δ* cells (yAV1107) containing *RRP40-Myc* (pAC3161), *rrp40-G8A-Myc* (pAC3162), *rrp40-S87A-Myc* (pAC3257), *rrp40-W195A-Myc* (pAC3163), or rrp40-W195R-Myc (pAC3259) plasmid and *his3-nonstop* (pAV188) plasmid (van Hoof *et al.* 2002), encoding a His3-nonstop reporter, were serially diluted and spotted onto Ura$^-$ and Ura$^-$ His$^-$ minimal medium plates and grown at 37°. As a control, *ski7Δ* (yAV571) cells containing *his3-nonstop* plasmid (pAV188) were also assayed for growth on Ura$^-$ and Ura$^-$ His$^-$ minimal medium plates.

Total RNA isolation

To prepare *S. cerevisiae* total RNA from cell pellets of 10 ml cultures grown to OD_{600} = 0.5–0.8, cell pellets in 2 ml screw-cap tubes were resuspended in 1 ml TRIzol (Invitrogen), 300 μl glass beads were added, and cell samples were disrupted in Mini Bead Beater 16 Cell Disrupter (Biospec) for 2 min at 25°. For each sample, 100 μl of 1-bromo-3-chloropropane (BCP) was added, the sample was vortexed for 15 sec, and incubated at 25° for 2 min. Sample was centrifuged at 16,300 × *g* for 8 min at 4°, and the upper layer was transferred to a fresh microfuge tube. RNA was precipitated with 500 μl isopropanol, and the sample was vortexed for 10 sec to mix. Total RNA was pelleted by centrifugation at 16,300 × *g* for 8 min at 4°. RNA pellet was washed with 1 ml of 75% ethanol, centrifuged at 16,300 × *g* for 5 min at 4°, and air-dried for 15 min. Total RNA was resuspended in 50 μl diethylpyrocarbonate (DEPC, Sigma)-treated water, and stored at −80°.

Quantitative RT- PCR

For analysis of *NEL025c* CUT, *U4* snRNA, and *ITS-2* rRNA levels in *rrp40* mutant cells, *rrp40Δ* (yAV1107) cells containing *RRP40-Myc* (pAC3161), *rrp40-G8A* (pAC3162), or *rrp40-W195R-Myc* (pAC3259) were grown in 2 ml Leu$^-$ minimal medium overnight at 30°, 10 ml cultures with an OD_{600} = 0.4 were prepared and grown at 37° for 5 hr. Cells were collected by centrifugation (2163 × *g*), transferred to 2 ml screw cap tubes and stored at −80°. Following total RNA isolation from each cell pellet, 1 μg RNA was reverse transcribed to first strand cDNA using the M-MLV Reverse Transcriptase (Invitrogen) according to the manufacturer's protocol. Quantitative PCR was performed on technical triplicates of cDNA (10 ng) from three independent biological replicates using *NEL025c*, *U4*, *ITS-2* primers and control

ALG10 primers (0.5 μM; Table S2), and QuantiTect SYBR Green PCR master mix (Qiagen) on a StepOnePlus Real-Time PCR machine (Applied Biosystems; T_{anneal}: 55°; 44 cycles). The mean RNA levels were calculated by the ΔΔCt method (Livak and Schmittgen 2001), normalized to mean RNA levels in *RRP40* cells, and converted and graphed as RNA fold change relative to *RRP40*, with error bars that represent the SD from the mean.

Immunoblotting

For analysis of C-terminally Myc-tagged Rrp40 and rrp40 protein expression levels, *rrp40Δ* cells (yAV1107) or *RRP40-TAP* cells expressing Rrp40-Myc (pAC3161), rrp40-G8A-Myc (pAC3162), rrp40-S87A (pAC3257), rrp40-W195R-Myc (pAC3259), rrp40-W195A-Myc (pAC3163), or rrp40-W195F-Myc (pAC3286) protein, or containing vector (pRS315) were grown in 2 ml Leu$^-$ minimal medium overnight at 30° to saturation, and 10 ml cultures with an OD_{600} = 0.4 were prepared and grown at 30 and 37° for 5 hr. Cell pellets were collected by centrifugation, transferred to 2 ml screw-cap tubes and stored at −80°. For analysis of EXOSC3 expression levels, mouse N2a cells (Klebe and Ruddle 1969) were transiently transfected with bicistronic CMV-IRES-*EGFP* vector (pIGneo) containing *Myc-Exosc3* (pAC3417), *Myc-Exosc3^{G31A}* (pAC3418), or *Myc-Exosc3^{W237R}* (pAC3420) plasmid using Lipofectamine 2000 (Invitrogen), and cells were collected 24 hr after transfection.

Yeast cell lysates were prepared by resuspension of cells in 0.3 ml RIPA-2 Buffer (50 mM Tris-HCl, pH 8; 150 mM NaCl; 0.5% sodium deoxycholate; 1% NP40; 0.1% SDS) supplemented with protease inhibitors [1 mM PMSF; 3 ng/ml PLAC (pepstatin A, leupeptin, aprotinin, and chymostatin)], addition of 300 μl glass beads, disruption in a Mini Bead Beater 16 Cell Disrupter (Biospec) for 4 × 1 min at 25°, and centrifugation at 16,000 × *g* for 20 min at 4°. Mouse N2a cell lysates were prepared by lysis in RIPA-2 Buffer, and centrifugation at 16,000 × *g* for 10 min at 4°. Protein lysate concentration was determined by Pierce BCA Protein Assay Kit (Life Technologies). Whole cell lysate protein samples (20–50 μg) were resolved on Criterion 4–20% gradient denaturing gels (Bio-Rad), transferred to nitrocellulose membranes (Bio-Rad) and Myc-tagged Rrp40 and EXOSC3 proteins were detected with anti-Myc monoclonal antibody 9B11 (1:2000; Cell Signaling), TAP-tagged Rrp40 protein was detected with peroxidase anti-peroxidase (PAP) antibody (1:5000; Sigma). As loading controls, 3-phosphoglycerate kinase (Pgk1) protein was detected with anti-Pgk1 monoclonal antibody (1:30,000; Invitrogen), and eIF5A protein was detected with a rabbit anti-eIF5A polyclonal antibody (1:5000; Santa Cruz Biotechnology). For transfection control, GFP from pIGneo bicistronic *EGFP-Myc-Exosc3* vectors was detected with anti-GFP monoclonal antibody (1:5000; Santa Cruz Biotechnology).

Protein stability assay

To determine the stability of wild-type Rrp40-Myc and rrp40-Myc variant in *rrp40Δ* (yAV1107), wild-type (MHY501) or *doa3-1* (MHY3646) cells expressing Rrp40-Myc (pAC3161), rrp40-G8A (pAC3162), or rrp40-W195R (pAC3259), were grown in 10 ml Leu$^-$ minimal medium overnight at 30°, and 200 ml cultures with an OD_{600} = 0.4 were prepared. *rrp40Δ* (yAV1107) and *RRP40-TAP* cultures were grown for 2 hr at 30 or 37° and wild-type (MHY501) and *doa3-1* (MHY3646) cultures were grown at 37° for 2 hr. Cycloheximide (CHX, Sigma) was added to the cultures at a final concentration of 100 μg/ml. Samples (20 ml) were taken immediately after CHX addition at 0 time point. *rrp40Δ* and *RRP40-TAP* cultures were grown at 30° or 37°, and wild-type and *doa3-1* cultures were grown at 37° and 20 ml samples were collected at 5–35 min time points every 5 min, or 0.5–4.5 hr every 30 min. Cell sample pellets were collected by centrifugation, transferred to 2 ml screw cap tubes and stored at –80°. Protein lysates from cell sample pellets were prepared by resuspension of cells in 0.3 ml RIPA-2 Buffer supplemented with protease inhibitors (as above), addition of 300 μl glass beads, disruption in a Mini Bead Beater 16 Cell Disrupter (Biospec) for 4 × 1 min at 25°, and centrifugation at 16,000 × *g* for 20 min at 4°. Protein lysate concentration was determined by Pierce BCA Protein Assay Kit (Life Technologies). Protein lysate (30 μg) from each time point was analyzed by denaturing SDS-PAGE and immunoblotting with anti-Myc monoclonal antibody to detect Myc-tagged Rrp40 and rrp40 proteins, and anti-Pgk1 monoclonal antibody to detect Pgk1 as a loading control.

Quantitation of immunoblots

The band intensities/areas from all immunoblots were quantitated using ImageJ v1.4 software (National Institutes of Health, MD; http://rsb.info.nih.gov/ij/), and relevant percentages of protein were calculated in Microsoft Excel for Mac 2011 (Microsoft Corporation). To quantitate the percentage of rrp40-Myc variant relative to wild-type Rrp40-Myc protein in *rrp40Δ* cell and *RRP40-TAP* cells, rrp40-Myc intensity was normalized to Pgk1 intensity and Rrp40-Myc intensity. To quantitate and graph the relative intensity of Rrp40-TAP protein and wild-type Rrp40-Myc protein, or rrp40-Myc variant, in *RRP40-TAP* cells, the Rrp40-TAP and R/rrp40-Myc intensity was normalized to Pgk1 intensity, and the relative intensities of Rrp40-TAP and R/rrp40-Myc were graphed as two stack columns using Microsoft Excel. To quantitate the percentage of Myc-EXOSC3 variant relative to wild-type Myc-EXOSC3 protein, Myc-EXOSC3 variant intensity was normalized to GFP intensity and Myc-EXOSC3 intensity. In the Rrp40 protein stability assays, to quantitate the percentage remaining of wild-type Rrp40-Myc protein or rrp40-Myc variant in *rrp40Δ*, *RRP40-TAP*, wild-type, or *doa3-1* cells at each time point relevant to time 0, Rrp40-Myc or rrp40-Myc protein intensity at each time point was normalized to Pgk1 intensity and Rrp40-Myc, or rrp40-Myc, protein intensity at time 0. For the exponential decay curves, these Rrp40 protein percentages were plotted and best fit/least-squares exponential curves were calculated using Microsoft Excel. For the inset graphs, the natural logarithm (ln) of

Rrp40 protein percentages at each time point were plotted and fitted with least-squares lines using Microsoft Excel. All best fit lines had reasonable correlation coefficients (R^2 = 0.89–0.99). The slopes of the best fit lines were calculated to determine the decay rate constants (k) for the Rrp40 proteins, and the half-lives ($t_{1/2}$) of the Rrp40 proteins were calculated using the equation $t_{1/2} = \ln(2)/k$ as previously used to determine protein half-lives (Belle *et al.* 2006). The quantitation is for specific experiments shown in figures, but is representative of multiple experiments.

Blue native-PAGE

Blue native-PAGE (BN-PAGE) was performed essentially as described in a published protocol (Wittig *et al.* 2006). For analysis of wild-type Rrp40-Myc and rrp40-Myc variants expressed in *S. cerevisiae* cells by BN-PAGE, wild-type (MHY501), *doa3-1* (MHY3646), or *rrp40Δ* cells (yAV1107) cells expressing Rrp40-Myc (pAC3161), rrp40-G8A-Myc (pAC3162), rrp40-S87A (pAC3257), or rrp40-W195R-Myc (pAC3259) protein were grown in 2 ml Leu$^-$ minimal medium overnight at 30° to saturation, and 10 ml cultures with an OD_{600} = 0.4 were prepared; wild-type and *doa3-1* cells were grown at 37°, and *rrp40Δ* cells at 30° for 5 hr. Cell pellets were collected by centrifugation, transferred to 2 ml screw-cap tubes and stored at −80°. Yeast cell lysates were prepared by resuspension of cells in 0.3 ml IPP150 Buffer (10 mM Tris-HCl, pH 8; 150 mM NaCl; 0.1% NP40) supplemented with protease inhibitors [1 mM PMSF; 3 ng/ml PLAC (pepstatin A, leupeptin, aprotinin, and chymostatin)], addition of 300 μl glass beads, disruption in a Mini Bead Beater 16 Cell Disrupter (Biospec) for 4 × 1 min at 25°, and centrifugation at 16,000 × *g* for 20 min at 4°. Whole cell lysate protein samples (20–50 μg) were mixed with nondenaturing loading dye and resolved on Criterion 4–20% gradient BN-PAGE gels (Bio-Rad). The upper chamber of the electrophoresis apparatus contained Cathode buffer B (50 mM Tricine; 7.5 mM Imidazole; 0.2% Coomassie blue G-250; pH 7), and the lower chamber contained Anode buffer (25 mM Imidazole, pH 7), and the BN-PAGE gel was resolved at 100 V for 2–3 hr at 4°. The proteins were transferred to PDVF membranes (Bio-Rad) in transfer buffer (50 mM Tricine; 7.5 mM Imidazole; pH 7) at 20 V for 3 hr at 4°. Myc-tagged Rrp40 and rrp40 proteins were detected with anti-Myc monoclonal antibody, and the Pgk1 protein was detected with anti-Pgk1 monoclonal antibody as a loading control.

Glycerol gradient fractionation

For analysis of wild-type Rrp40-Myc and rrp40-W195R-Myc variants expressed in *S. cerevisiae* cells by glycerol gradient fractionation, *doa3-1* (MHY3646) cells expressing Rrp40-Myc (pAC3161) or rrp40-W195R-Myc (pAC3259) protein were grown in 10 ml Leu$^-$ minimal medium overnight at 30° to saturation, and 200 ml *doa3-1* cultures with an OD_{600} = 0.4 were prepared and grown at 37° for 5 hr. Cell pellets were collected by centrifugation, transferred to 2 ml screw-cap tubes, and stored at −80°. Yeast cell lysates were prepared by resuspension of cells in 0.5 ml native lysis buffer [10 mM HEPES, pH 7.5; 2 mM $MgCl_2$; 10 mM KCl; 0.5% NP-40; 0.5 mM EDTA; 150 mM NaCl; 1 mM DTT; Complete Protease Inhibitor Cocktail (Invitrogen)], addition of 300 μl glass beads, disruption in a Mini Bead Beater 16 Cell Disrupter (Biospec) for 4 × 1 min at 25°, and centrifugation at 16,000 × *g* for 20 min at 4°. Cell lysate (2 mg) was layered on top of a 10–30% glycerol gradient buffer [10 mM HEPES, pH 7.5; 2 mM $MgCl_2$; 10 mM KCl; 0.5 mM EDTA; 150 mM NaCl] in 14 × 89 mm tubes (Beckman Coulter) and centrifuged in a SW 41 Ti swinging-bucket rotor (Beckman Coulter) at 134,000 × *g* for 12 hr at 4°. Gradients were fractionated as 500 μl fractions from top to bottom. Every other fraction (40 μl) was analyzed by SDS-PAGE and immunoblotting with anti-Myc monoclonal antibody to detect Myc-tagged Rrp40 and rrp40-W195R, and anti-Pgk1 monoclonal antibody to detect Pgk1 as a loading control.

Data availability

The authors state that all data necessary for confirming the conclusions presented in the article are represented fully within the article. All strains and plasmids employed are available upon request.

Results

PCH1b patients have mutations that alter conserved EXOSC3 residues

PCH1b is caused by mutations in the *EXOSC3* exosome cap subunit gene (Wan *et al.* 2012), but, thus far, only a few specific amino acid substitutions have been definitively linked to PCH1b (Figure 1, B and C). Specifically, PCH1b patients homozygous for *EXOSC3* (G31A) have a severe disease, while patients homozygous for *EXOSC3* (D132A) have a less severe disease (Figure 1C) (Wan *et al.* 2012; Biancheri *et al.* 2013; Rudnik-Schoneborn *et al.* 2013; Schwabova *et al.* 2013; Eggens *et al.* 2014). *EXOSC3* (D132A) has also been found in compound heterozygosity with likely null alleles in PCH1b patients with severe disease (Wan *et al.* 2012; Rudnik-Schoneborn *et al.* 2013; Eggens *et al.* 2014). On the other hand, *EXOSC3* (G31A) has not been found in combination with obvious null alleles, but it has been found in compound heterozygosity with *EXOSC3* (W238R) (Wan *et al.* 2012; Rudnik-Schoneborn *et al.* 2013). Although loss of *EXOSC3* has been modeled in zebrafish by knockdown with antisense morpholinos (Wan *et al.* 2012), the functional consequences of specific amino acid substitutions in EXOSC3 have not previously been analyzed in detail.

To begin to analyze specific PCH1b-associated amino acid substitutions in EXOSC3, we generated a protein sequence alignment of human EXOSC3, the budding yeast EXOSC3 ortholog, Rrp40, and other eukaryotic EXOSC3/Rrp40 orthologs (Figure S1). The human RNA exosome subunit EXOSC2 is similar to EXOSC3, so we also included human EXOSC2 and its budding yeast ortholog, Rrp4, in the alignment. As

EXOSC2 and EXOSC3 are replaced by Rrp4 in Archaea (Buttner *et al.* 2005; Lorentzen *et al.* 2007), we also aligned archaeal Rrp4. Human EXOSC3 residues substituted in PCH1b are among the most conserved residues in this protein (Figure S1). Only 10 human EXOSC3 residues are perfectly conserved in the sequences analyzed, and two of these conserved residues are the PCH1b-associated EXOSC3 residues, G31 and W238 (Figure S1 and Figure 1B). EXOSC3 residue D132 is also conserved in most EXOSC3/Rrp40 orthologs, but it is replaced by serine in budding yeast Rrp40 and most other ascomycete fungi Rrp40 orthologs (Figure S1 and Figure 1B). The EXOSC3/Rrp40 protein contains three domains: an N-terminal domain, an S1 putative RNA binding domain, and a KH putative RNA binding domain (Figure 1B). Notably, the human EXOSC3-G31/budding yeast Rrp40-G8 residue is located in the N-terminal domain, EXOSC3-D132/Rrp40-S87 residue is located in the S1 domain, and EXOSC3-W238/Rrp40-W195 residue is located in the KH domain (Figure 1B).

To assess the potential interactions of PCH1b-associated EXOSC3/Rrp40 residues, we examined both human and budding yeast RNA exosome structures (Liu *et al.* 2006; Makino *et al.* 2013; Wasmuth *et al.* 2014) (Figure 1D). Based on these structures, the positions of the PCH1b-associated conserved residues (black, bold) in EXOSC3/Rrp40 (blue) are shown within the context of the RNA exosome (Figure 1D). Strikingly, although PCH1b-associated EXOSC3/Rrp40 residues are not clustered together in primary sequence, and are located in different EXOSC3/Rrp40 domains (Figure 1B) (Wan *et al.* 2012), the residues are all in positions that could be important for interactions with other RNA exosome subunits. Specifically, Rrp40 residue G8 is packed against Rrp46 residues S129, M130, and V168 (Figure 1D). Substituting any bulkier side chain at Rrp40 G8, including substitution to alanine corresponding to the PCH1b-associated G31A substitution, could interfere with Rrp40-Rrp46 interaction. Rrp40 residue S87 forms a hydrogen bond with Rrp40 Q89 (Figure 1D), which could be disrupted by S87A substitution in Rrp40 corresponding to the PCH1b-associated D132A substitution in EXOSC3. In the human exosome structure, the corresponding EXOSC3 residue D132 appears to form a hydrogen bond with EXOSC3 G134 (Figure 1D). Disrupting this hydrogen bond could impair the folding of a loop within the Rrp40/EXOSC3 S1 domain. Unlike Rrp40 residues G8 and S87, Rrp40 W195 is not located at an exosome subunit interface, but could still be important intersubunit interactions. Rrp40 W195 is located in a pocket surrounded by a loop containing Rrp40 D152, which is positioned to make a salt bridge to Rrp45 K13. In the human exosome structure, although not identically positioned, the corresponding EXOSC3 residue W238 is located in a pocket near EXOSC3 D196 and EXOSC9 R12. The Rrp40 W195R substitution could therefore alter the position of D152, which could weaken interaction with Rrp45. In addition to interactions with other exosome subunits, the PCH1b-associated EXOSC3/Rrp40 residues could also lie in close proximity to RNA or could contribute to interactions with RNA exosome cofactors.

We used the budding yeast *S. cerevisiae* to begin to assess the functional consequences of the PCH1b-associated EXOSC3-G31A, -D132A, and -W238R substitutions because these residues are highly conserved in EXOSC3/Rrp40 orthologs, and located in key structural EXOSC3/Rrp40 domains. Furthermore, the budding yeast RNA exosome has been extensively characterized, and is similar to the human RNA exosome (Sloan *et al.* 2012). As illustrated in Figure 1B, we created mutations in the budding yeast *RRP40* gene that result in the following rrp40 amino acid substitution variants: rrp40-G8A (corresponding to EXOSC3-G31A); rrp40-S87A (corresponding to D132A); and rrp40-W195R (corresponding to W238R). These rrp40 variants were used to assess the functional consequences of these substitutions in the Rrp40 exosome subunit.

Amino acid substitutions in Saccharomyces cerevisiae Rrp40 corresponding to PCH1b-associated EXOSC3 substitutions impair function

In budding yeast, all of the core RNA exosome subunits are encoded by essential genes (Allmang *et al.* 1999). As a first test of the functional consequences of PCH1b-associated substitutions, we assessed whether the *rrp40* mutant genes could complement the lethality of a yeast *rrp40*Δ mutant. For these studies, we examined the rrp40-G8A, rrp40-S87A, and rrp40-W195R variants (Figure 2). As the change of tryptophan 195 to arginine in rrp40-W195R is a dramatic change, we also changed tryptophan 195 to alanine (rrp40-W195A) to remove the large hydrophobic residue without simultaneously introducing a positive charge. In addition, we created a very conservative change of tryptophan 195 to phenylalanine (rrp40-W195F), which retains the large hydrophobic residue.

We grew *rrp40Δ* cells expressing each rrp40 substitution variant as the sole copy of the essential Rrp40, serially diluted and spotted the cells on plates, and incubated the plates at various temperatures (Figure 2A). In this solid medium endpoint assay, *rrp40-W195R* and *rrp40-W195A* mutant cells gave rise to smaller colonies at 37°, indicative of a modest growth defect that is most noticeable on day 1 of growth. To provide a more quantitative comparison of growth rates, we also performed growth assays in liquid cultures at 37° (Figure 2B and Figure S2). This analysis revealed that *rrp40-W195R* and *rrp40-W195A* mutant cells grow at a slower rate than wild-type *RRP40* cells, with doubling times increased by 13 and 20%, respectively, compared to *RRP40* cells (Figure 2B and Figure S2A). The other *rrp40* mutants analyzed, *rrp40-G8A* and *rrp40-S87A*, grew in a manner indistinguishable from wild-type *RRP40* cells (Figure 2B). The *rrp40-W195F* mutant also grew similarly to wild-type *RRP40* cells (Figure S2B). At 30°, the *rrp40-W195R* and *rrp40-W195A* mutant cells also reproducibly grew more slowly than the other mutants, although the difference was less pronounced than at 37°. In a plasmid shuffle assay, in which *rrp40Δ* cells containing an *RRP40 URA3* maintenance plasmid and each *rrp40* mutant were grown on 5-FOA plates at several temperatures to select against the maintenance plasmid, the

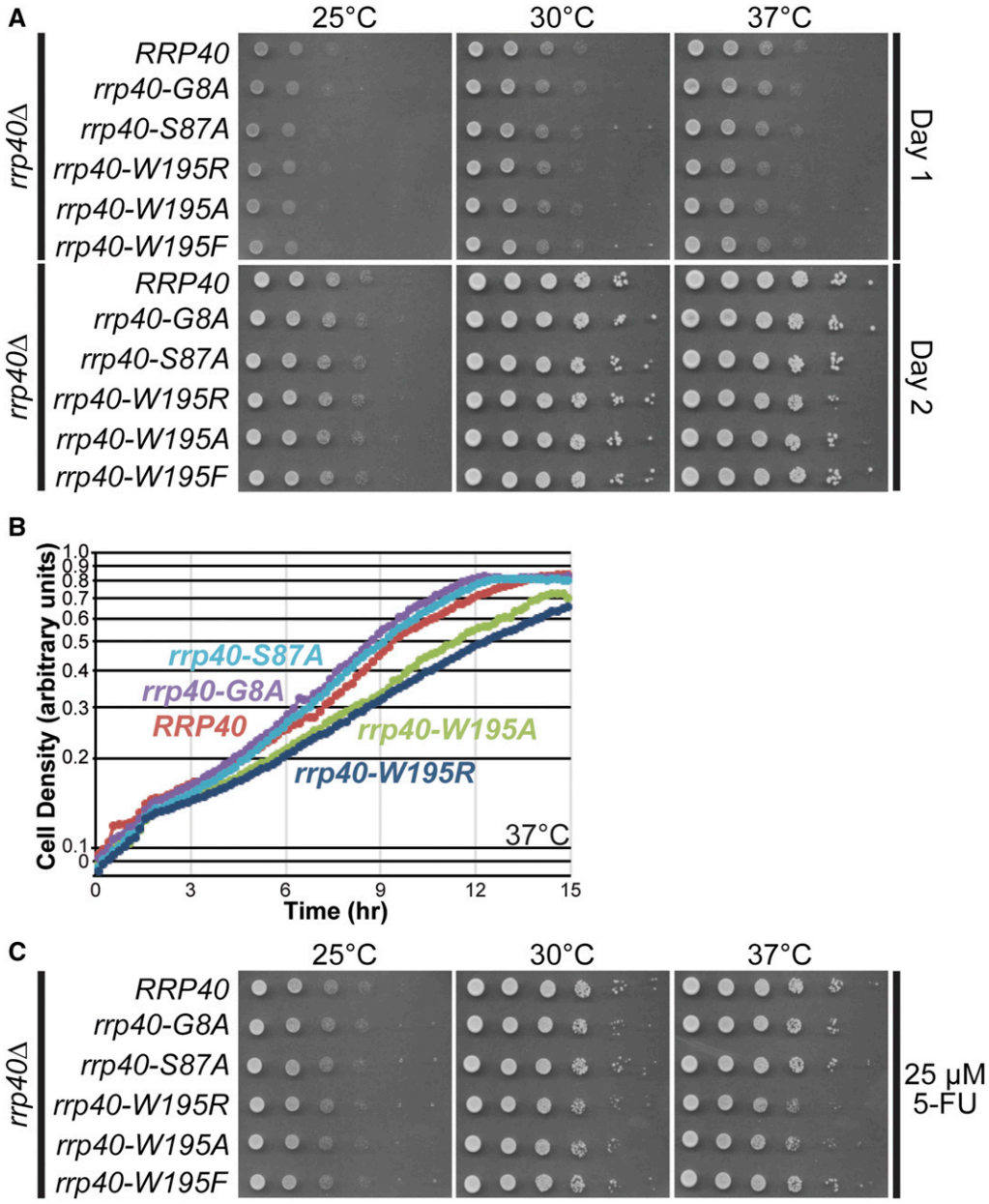

Figure 2 S. *cerevisiae* cells that express rrp40-W195R or rrp40-W195A as the sole copy of Rrp40 show impaired growth at 37°. Growth of *rrp40Δ* cells containing only wild-type *RRP40* or mutant *rrp40* (*G8A*, *S87A*, *W195R*, *W195A*, or *W195F)* plasmid was analyzed by: (A) Serial dilution, spotting on minimal medium plates, and growth at indicated temperatures for 1 day (Day 1) or 2 days (Day 2). (B) Growth in liquid culture at 37° and optical density measurements over time. (C) Serial dilution, spotting on minimal medium plates containing 5-FU, and growth at indicated temperatures.

rrp40-W195R and *rrp40-W195A* mutant cells also showed slow growth at 30 and 37°, whereas *rrp40-W195F* cells showed no growth defect (Figure S3).

We took advantage of the fact that the exosome mutants, such as *rrp6Δ*, are sensitive to the antimetabolite 5-FU, an inhibitor of thymidine synthesis that impairs both DNA and RNA metabolism (Fang *et al.* 2004; Lum *et al.* 2004). To further assess the function of rrp40-W195R and rrp40-W195A, we serially diluted and spotted *rrp40* mutants on solid medium plates containing 5-FU, and incubated the plates at several temperatures (Figure 2C). The *rrp40-W195R* and *rrp40-W195A* mutant cells show reduced growth on 5-FU plates at 37° relative to wild-type *RRP40* cells. In contrast, the *rrp40-W195F* mutant cells show growth similar to *RRP40* cells. These results demonstrate that no single amino acid substitution in Rrp40, corresponding to a PCH1b-associated substitution in EXOSC3, causes a complete loss of Rrp40 function, and that substitutions that remove the large hydrophobic W195 residue modestly impair cell growth. These results are not surprising as Rrp40 is essential in budding yeast (http://www.yeastgenome.org), and loss of EXOSC3 is embryonic lethal in mice (http://www.mousephenotype.org); thus, some threshold level of function is likely required in EXOSC3 for viability and development in humans.

The rrp40-W195R mutant exhibits elevated levels of exosome RNA targets

To assess whether the slow growth observed for the *rrp40-W195R* mutant correlates with a change in RNA exosome

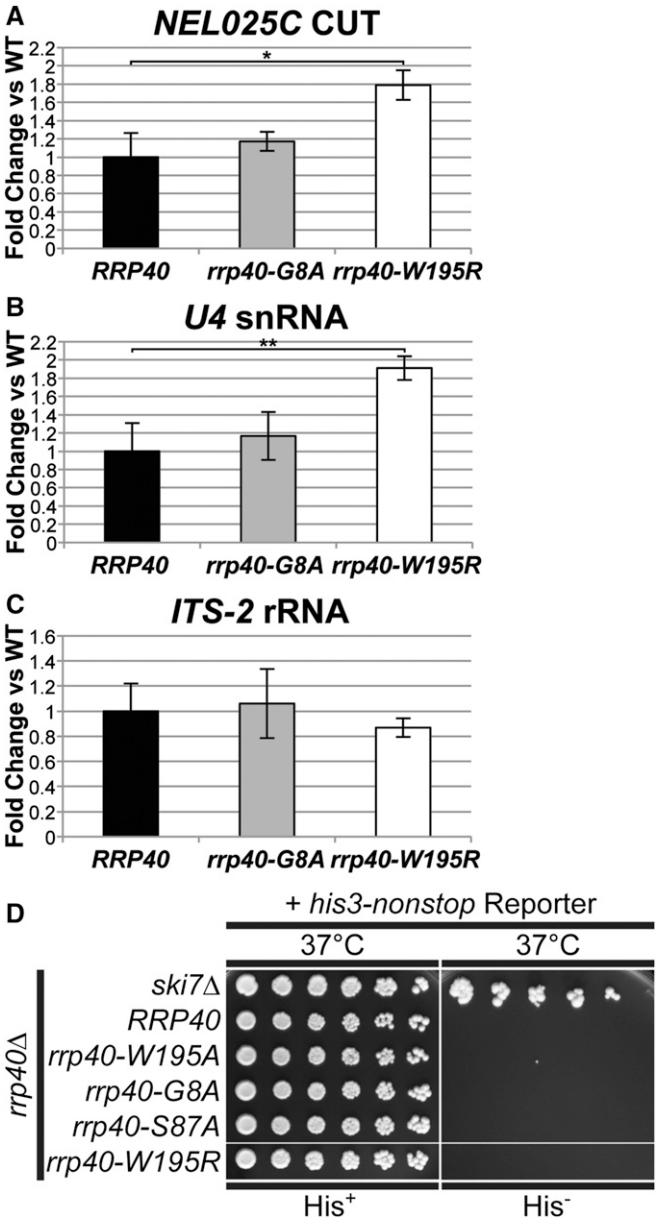

Figure 3 The rrp40-W195R mutant cells show elevated levels of exosome target transcripts but do not exhibit impaired cytoplasmic exosome function. (A–C) The *rrp40-W195R* mutant cells show a statistically significant increase in the levels of noncoding RNAs, (A) *NEL025c* CUT and (B) *U4* snRNA, but not (C) *ITS-2* rRNA, at 37°. Total RNA from *rrp40Δ* cells containing only wild-type *RRP40* or mutant *rrp40* (*G8A*; *W195R*) grown at 37° was measured by quantitative RT-PCR using *NEL025c* CUT, *U4* snRNA, and *ITS-2* rRNA primers as described in *Material and Methods*. Relative RNA levels were measured in triplicate biological samples, normalized to a control *ALG10* transcript by the ΔΔCt method, averaged, and shown graphically as fold increase relative to wild-type *RRP40*. Error bars denote SD. The difference in *NEL025c* CUT levels between rrp40-W195R and wild-type cells is significant ($P = 0.0114$; denoted by *) and the difference in *U4* snRNA levels between rrp40-W195R and wild-type cells is very significant ($P = 0.0090$; denoted by **). The differences in RNA levels between rrp40-G8A and wild-type cells are not significant. Statistically significant differences in mean RNA levels were determined using the unpaired *t*-test. (D) The *rrp40* mutant cells do not rescue a *his3-nonstop* mRNA reporter, which is degraded rapidly by the cytoplasmic RNA exosome (van Hoof *et al.* 2002), to restore growth on medium lacking histidine, suggesting that *rrp40* mutants do not impact cytoplasmic RNA exosome function. As a control, deletion of *SKI7*, encoding a key cytoplasmic RNA exosome cofactor (van Hoof *et al.* 2000), rescues the *his-nonstop* reporter and thus confers growth on medium lacking histidine. The *rrp40Δ* cells containing wild-type *RRP40* or mutant *rrp40* (G8A; S87A; W195R; W195A) plasmid and the *his3-nonstop* mRNA reporter plasmid, and *ski7Δ* cells containing the *his3-nonstop* mRNA reporter plasmid were serially diluted and spotted onto minimal medium plates lacking histidine (His$^-$) or control plates containing histidine (His$^+$) and grown at 37°.

function, we examined the steady-state level of several well defined RNA exosome target transcripts, the *NEL025C* cryptic unstable transcript (CUT), *U4* snRNA, and *ITS2* rRNA (Wasmuth and Lima 2012). Levels of *NEL025C* and *U4* RNA were modestly, but statistically significantly, increased in *rrp40-W195R* mutant cells at 37° (Figure 3, A and B), consistent with the change in cell growth. The level of *ITS2* RNA was not changed significantly, suggesting that not all targets are affected equally (Figure 3C). No significant difference in the level of the RNA targets was detected in the *rrp40-G8A* mutant cells. These results provide further evidence that RNA exosome function is compromised in the *rrp40-W195R* mutant cells.

We next extended our analyses to assess whether these rrp40 variants affect the cytoplasmic functions of the RNA exosome. The rationale for examining cytoplasmic RNA exosome function is threefold: first, the cytoplasmic functions of the RNA exosome are nonessential, and thus distinct from those tested above (Jacobs Anderson and Parker 1998; Schaeffer *et al.* 2010); second, residue substitutions in a different RNA exosome cap protein (Csl4/EXOSC1) inactivate cytoplasmic RNA exosome function without blocking the essential (nuclear) function (van Hoof *et al.* 2000); and third, the hypothesis has been put forth that PCH1b and PCH1c are the result of a defect in cytoplasmic mRNA degradation by the RNA exosome (Boczonadi *et al.* 2014).

To examine cytoplasmic exosome function in *rrp40* mutants, we employed a *his3-nonstop* reporter assay that exploits the observation that the budding yeast cytoplasmic RNA exosome is required for the degradation of mRNAs that lack stop codons (van Hoof *et al.* 2002). In cells with functional cytoplasmic exosome, the *his3-nonstop* mRNA reporter, which encodes the His3 protein and lacks stop codons, is degraded, no histidine is made, and the cells cannot grow on media lacking histidine. In cells with defective cytoplasmic RNA exosome, the *his3-nonstop* mRNA reporter is stabilized, biosynthesis of histidine proceeds, and cells can grow on media lacking histidine. The *rrp40Δ* cells expressing each rrp40 variant as the sole copy of Rrp40, and containing the *his3-nonstop* reporter, were serially diluted and spotted onto solid medium lacking histidine (His$^-$) and control medium containing histidine (His$^+$) (Figure 3D). As a control for impaired cytoplasmic exosome function, we also diluted and spotted a *ski7Δ* strain containing the *his3-nonstop* reporter, as Ski7 is a cofactor required for cytoplasmic exosome

function (van Hoof *et al.* 2002). As expected, the *ski7Δ* control strain grew on His$^-$ medium (Figure 3D). In contrast, none of the experimental *rrp40* mutants grew on His$^-$ medium, indicating that cytoplasmic exosome-mediated nonstop mRNA decay proceeds normally in cells expressing these rrp40 variants (Figure 3D). These results suggest that amino acid substitutions linked to PCH1b do not block the function of the cytoplasmic RNA exosome, at least in the budding yeast system.

The rrp40-W195R variant is expressed at low level and is unstable when expressed as the sole copy of Rrp40

To test whether amino acid substitutions in Rrp40 corresponding to those in PCH1b-associated EXOSC3 impact protein levels, we analyzed the steady-state expression of Myc-tagged wild-type Rrp40, rrp40-W195R, and the other rrp40 variants as the sole copy of Rrp40 in *rrp40Δ* cells grown at 30 and 37° by immunoblotting (Figure 4A). The steady-state level of the rrp40-W195R variant was reduced about threefold, whereas the levels of rrp40-S87A and rrp40-G8A variants were within twofold of wild-type Rrp40 at 37° (Figure 4A). The level of the rrp40-W195A variant, which also caused slow growth, was also reduced (57% of wild-type level) at 37° (Figure 4A). In contrast, the conservative rrp40-W195F variant level was modestly reduced (71% of wild-type level) (Figure 4A). These data indicate that the W195R substitution in Rrp40, corresponding to W238R in EXOSC3, strongly reduces the level of the protein at 37° and suggest the rrp40-W195R variant may be less stable than wild-type Rrp40.

To examine the stability of the rrp40-W195R variant, we analyzed the levels of the Myc-tagged rrp40-W195R and wild-type Rrp40 proteins expressed in *rrp40Δ* cells over time at 37° after cycloheximide treatment (Figure 4B). The exponential decay curves from these data reveal that the rrp40-W195R variant is unstable with a shorter half-life ($t_{1/2}$ ~85 min) compared to wild-type Rrp40 ($t_{1/2}$ ~131 min) at 37° (Figure 4C). We also examined the stability of the rrp40-W195R and rrp40-G8A variants at 30° (Figure S4), and found that rrp40-W195R is unstable ($t_{1/2}$ ~116 min), but the rrp40-G8A variant is stable ($t_{1/2}$ ~255 min), relative to wild-type Rrp40 ($t_{1/2}$ ~222 min) at 30°. These results indicate that the rrp40-W195R variant is unstable relative to wild-type Rrp40.

The rrp40-W195R variant is expressed at greatly reduced level when coexpressed with wild-type Rrp40 in an in vivo competition assay

A potential explanation for the reduced stability of the rrp40-W195R variant in *rrp40Δ* cells could be that the rrp40-W195R variant does not assemble efficiently into the exosome complex, and is therefore targeted for degradation by the proteasome. If this impaired exosome assembly model is correct, one prediction would be that the rrp40-W195R variant would be out-competed by wild-type Rrp40 for assembly into the exosome in an *in vivo* competition setting. We examined the expression of Myc-tagged wild-type Rrp40, and rrp40 variants, in *RRP40-TAP* cells that coexpress a tandem affinity purification (TAP)-tagged copy of wild-type Rrp40 at 30 and 37° by immunoblotting (Figure 5A). The steady-state levels of the rrp40-W195R and rrp40-W195A variants were decreased (to 24–30% of the wild-type level) in the *RRP40-TAP*

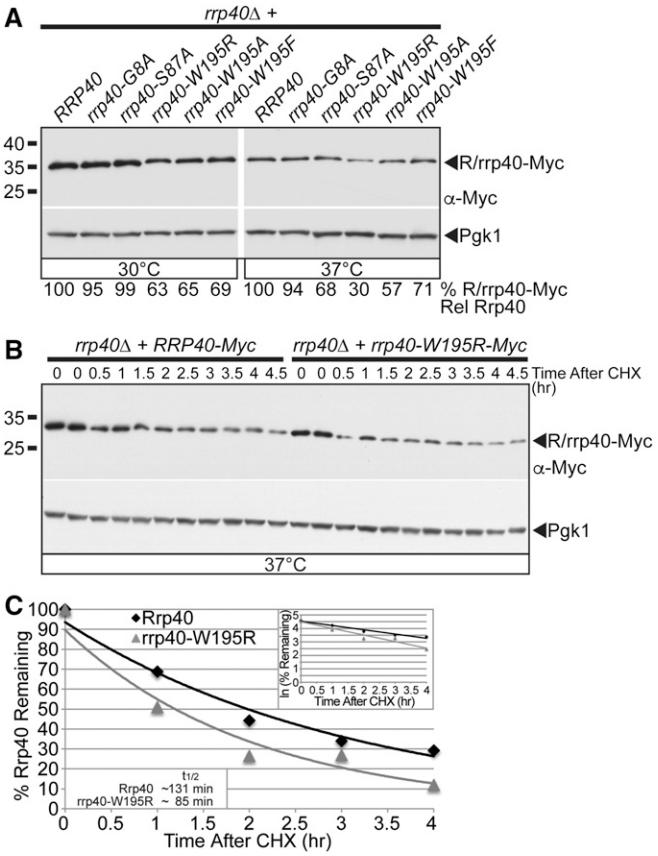

Figure 4 The rrp40-W195R variant is less stable than wild-type Rrp40 in cells as the only copy of Rrp40. (A) The steady-state level of the rrp40-W195R and rrp40-W195A variant is decreased compared to wild-type Rrp40 in *rrp40Δ* cells at 37°. Lysates of *rrp40Δ* cells expressing Myc-tagged wild-type Rrp40 or rrp40 variant (G8A, S87A, W195A, W195R, and W195F) grown at 30 or 37° were analyzed by immunoblotting with anti-Myc antibody to detect Myc-tagged Rrp40 and rrp40 variants (R/rrp40-Myc), and anti-Pgk1 antibody to detect Pgk1 as a loading control. The percentage of Rrp40-Myc or rrp40-Myc variant relative to wild-type Rrp40-Myc (% R/rrp40-Myc Rel Rrp40) is shown below each lane, and was calculated as described in *Materials and Methods*. (B) The rrp40-W195R variant is unstable in *rrp40Δ* cells at 37°. The *rrp40Δ* cells expressing Myc-tagged Rrp40 or rrp40-W195R were treated with the translation inhibitor CHX. Samples were collected over time (0–4.5 hr) and analyzed by immunoblotting with anti-Myc antibody to detect Myc-tagged Rrp40 and rrp40-W195R protein (R/rrp40-Myc), and anti-Pgk1 antibody to detect Pgk1 as a loading control. (C) The immunoblot shown in (B) was quantitated to plot the percentage of Rrp40 and rrp40-W195R protein remaining at each time point relative to inhibition of translation at time 0 in *rrp40Δ* cells. The inset graph shows the natural logarithm (ln)-transformed percentages of Rrp40 and rrp40-W195R at time points 0–4 hr fitted with linear least-squares fit lines to determine the decay rate constant (k) for each protein. The inset half-lives ($t_{1/2}$) of Rrp40 and rrp40-W195R in *rrp40Δ* cells at 37° were calculated from each decay rate constant using the equation $t_{1/2} = \ln(2)/k$ (Belle *et al.* 2006). Further details on the measurement of the percentages of protein using protein band intensities and calculation of the protein half-lives are described in *Materials and Methods*. Quantitation is for the specific experiment shown, but is representative of multiple experiments.

cells at both 30 and 37° (Figure 5A). However, the level of the conservative rrp40-W195F variant was much less affected (Figure 5A), suggesting that a large hydrophobic residue is required at position 195 in Rrp40. In contrast, the levels of rrp40-G8A and rrp40-S87A variants were similar to wild-type Rrp40 level (95–106%) (Figure 5A). Quantitation of the levels of Rrp40-Myc, rrp40-Myc variants, and Rrp40-TAP in the immunoblot show that, in *RRP40-TAP* cells with low levels of rrp40-W195R or rrp40-W195A variants, there was a high level of Rrp40-TAP, whereas in cells with high levels of rrp40-G8A-Myc or rrp40-S87A-Myc variant, there was a low level of Rrp40-TAP (Figure 5B). These data show that the level the rrp40-W195R variant is quite reduced in *RRP40-TAP* cells coexpressing wild-type Rrp40, and that the level of rrp40-W195R is much lower in *RRP40-TAP* cells (24% of wild-type level; Figure 5A) than it is in *rrp40Δ* cells (63% of wild-type level; Figure 4A) at 30°. These results suggest that the rrp40-W195R variant is more unstable in the presence wild-type Rrp40, and that rrp40-W195R cannot compete efficiently with wild-type Rrp40 for assembly into the exosome.

The rrp40-W195R variant is highly unstable, and rapidly degraded by the proteasome when coexpressed with wild-type Rrp40

To assess the stability of the rrp40-W195R variant in the presence of wild-type Rrp40, we examined the levels of Myc-tagged rrp40-W195R and Myc-tagged, wild-type Rrp40 in *RRP40-TAP* cells grown at 30° over time after cycloheximide treatment (Figure 6A). The exponential decay curves from these data reveal that the rrp40-W195R-Myc variant is highly unstable in *RRP40-TAP* cells with a very short half-life ($t_{1/2}$ ~6 min) compared to wild-type Rrp40-Myc at 30° (Figure 6B). In comparison, the half-life of rrp40-W195R-Myc in *rrp40Δ* cells at 30° was much longer ($t_{1/2}$ ~116 min), as described previously (Figure S4). This *in vivo* competition assay suggests that wild-type Rrp40 is assembled more efficiently in a stable RNA exosome complex than the rrp40-W195R variant.

We hypothesized that the rapid degradation of the rrp40-W195R variant in cells coexpressing wild-type Rrp40 is mediated by the proteasome. To directly test this hypothesis, we compared the stability of rrp40-W195R-Myc in wild-type cells with fully functional proteasome to *doa3-1* mutant cells expressing a temperature-sensitive variant of the Doa3 proteasome subunit (Li *et al.* 2007). Both wild-type and *doa3-1* cells also expressed endogenous, untagged, wild-type Rrp40. We examined the stability of rrp40-W195R in wild-type or *doa3-1* cells at 37° over time after cycloheximide treatment (Figure 6C). The stability of rrp40-W195R is greatly increased in *doa3-1* cells shifted to the nonpermissive temperature of 37°, where proteasome function is impaired compared to wild-type cells (Figure 6C). The exponential decay curves from these data reveal that rrp40-W195R is stable over the course of 35 min in *doa3-1* proteasome mutant cells, but is very unstable with a short half-life ($t_{1/2}$ ~5 min)

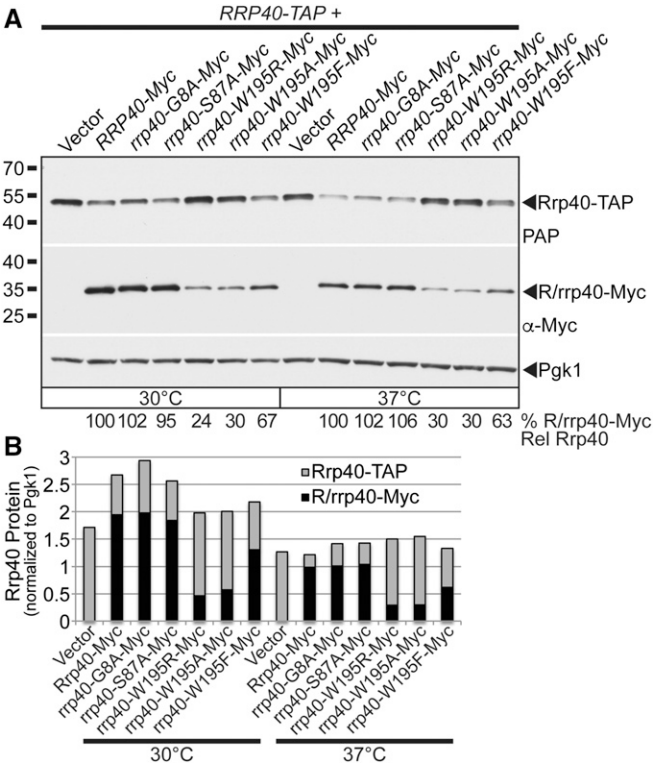

Figure 5 In an *in vivo* competition experiment, the rrp40-W195R-Myc variant is present at a greatly reduced level relative to wild-type Rrp40-Myc in cells coexpressing wild-type Rrp40-TAP. (A) rrp40-W195R-Myc and rrp40-W195A variants are expressed at lower steady-state levels compared to Rrp40-Myc in *RRP40-TAP* cells at 30 and 37°. Lysates of *RRP40-TAP* cells expressing wild-type Rrp40-Myc, or variant rrp40-Myc (G8A, S87A, W195R, W195A, and W195F) grown at 30 or 37° were analyzed by immunoblotting with anti-Myc antibody to detect Myc-tagged Rrp40 and rrp40 variants (R/rrp40-Myc), PAP antibody to detect Rrp40-TAP, and anti-Pgk1 antibody to detect Pgk1 as a loading control. The percentage of Rrp40-Myc and rrp40-Myc variant relative to wild-type Rrp40-Myc (% R/rrp40-Myc Rel Rrp40) is shown below each lane, and was calculated as described in *Materials and Methods*. (B) The immunoblot in (A) was quantitated to graph the relative intensity of wild-type Rrp40-Myc, variant rrp40-Myc, Rrp40-TAP protein bands in cells coexpressing R/rrp40-Myc and Rrp40-TAP at 30 and 37°. Cells with low levels of rrp40-W195R-Myc or rrp40-W195A-Myc variant have high levels of Rrp40-TAP. Cells with high levels of rrp40-G8A-Myc or rrp40-S87A variant have low levels of Rrp40-TAP. Further details on the measurement of the protein band intensities are described in *Materials and Methods*. Quantitation is for the specific experiment shown, but is representative of multiple independent experiments.

in wild-type cells (Figure 6D). These results indicate that the rrp40-W195R variant is degraded by the proteasome, and suggest that cells can selectively discriminate and target the rrp40-W195R variant for proteasome-mediated degradation when wild-type Rrp40 is available.

The rrp40-W195R variant associates less efficiently with the exosome complex when coexpressed with wild-type Rrp40

The reduced stability of the rrp40-W195R variant when coexpressed with wild-type Rrp40 could be explained by reduced assembly into the exosome complex. To examine the

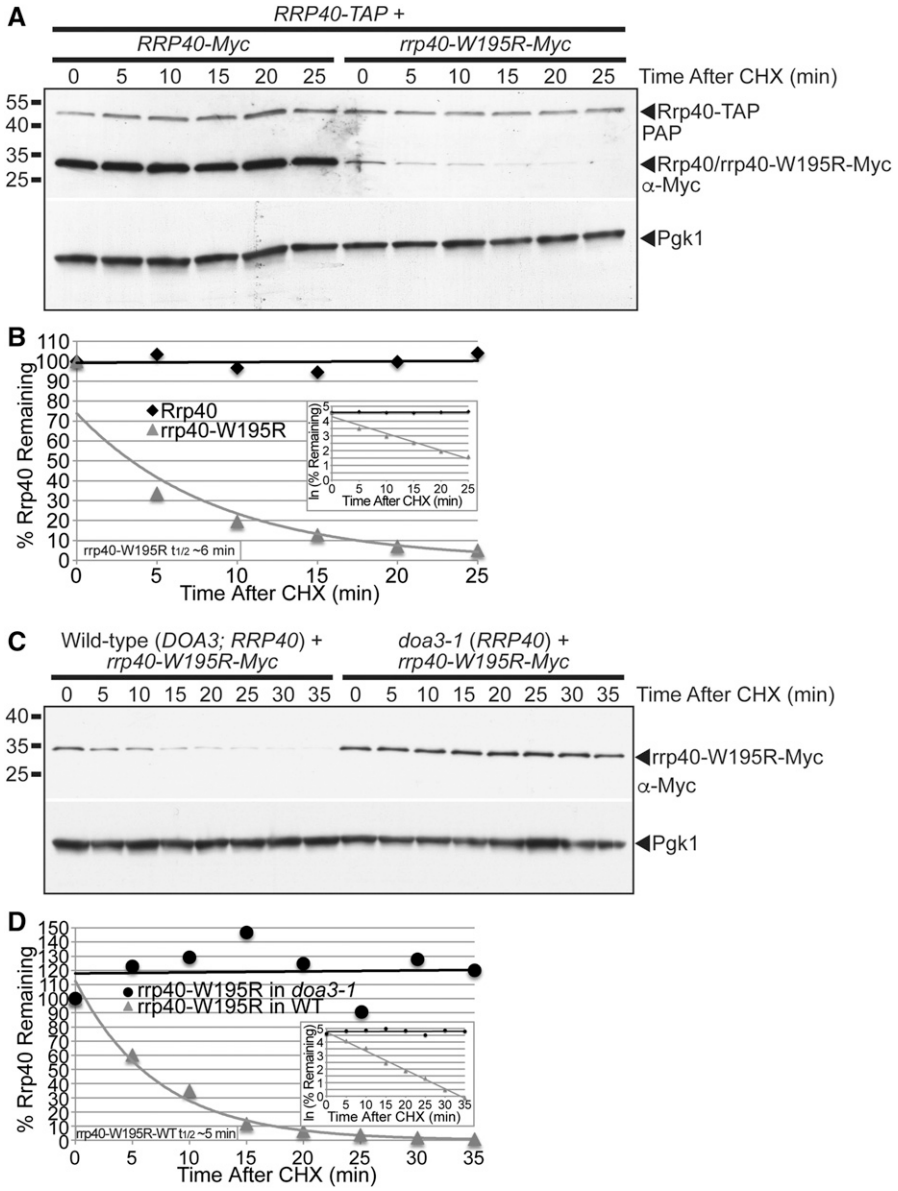

Figure 6 The rrp40-W195R variant is unstable and degraded by the proteasome in *S. cerevisiae* cells coexpressing wild-type Rrp40. (A) The level of rrp40-W195R-Myc variant decreases more rapidly than wild-type Rrp40-Myc over time in cells coexpressing wild-type Rrp40-TAP at 30°. *RRP40-TAP* cells expressing wild-type Rrp40-Myc or rrp40-W195R variant at 30° were treated with CHX to inhibit translation. Samples were collected over time (0–25 min) and analyzed by immunoblotting with anti-Myc antibody to detect Myc-tagged proteins (Rrp40/rrp40-W195R-Myc), peroxidase anti-peroxidase (PAP) antibody to detect Rrp40-TAP, and anti-Pgk1 antibody to detect Pgk1 as a loading control. (B) The immunoblot shown in (A) was quantitated to plot the percentage of Rrp40-Myc and rrp40-W195R-Myc protein remaining at each time point relative to inhibition of translation at time 0 in *RRP40-TAP* cells. The inset graph shows the natural logarithm (ln)-transformed percentages of Rrp40 and rrp40-W195R at time points 0–25 min fitted with linear least-squares fit lines to determine the decay rate constant (k) for each protein. The inset half-life ($t_{1/2}$) of rrp40-W195R in *RRP40-TAP* cells at 30° of ~6 min was calculated from the decay rate constant using the equation $t_{1/2} = \ln(2)/k$ (Belle *et al.* 2006). (C) The level of rrp40-W195R-Myc variant is increased in *doa3-1* proteasome mutant cells coexpressing wild-type Rrp40 at 37°. Wild-type or *doa3-1* cells expressing rrp40-W195R-Myc protein at 37° were treated with CHX. Samples were collected over time (0–35 min) and analyzed by immunoblotting with anti-Myc antibody to detect rrp40-W195R-Myc protein, and anti-Pgk1 antibody to detect Pgk1 as a loading control. (D) The immunoblot shown in (C) was quantitated to plot the percentage of rrp40-W195R-Myc protein at each time point in wild-type and *doa3-1* mutant cells. The inset graph shows the natural logarithm (ln)-transformed percentages of rrp40-W195R at time points 0–35 min in wild-type or *doa3-1* cells fitted with linear least-squares fit lines to determine the decay rate constant (k) for each protein. The inset half-life ($t_{1/2}$) of rrp40-W195R in wild-type cells at 30° of ~5 min was calculated as described in (B). Further details on the measurement of the protein band intensities and calculation of the protein half-lives are described in *Materials and Methods*. Quantitation is for the specific experiment shown, but is representative of multiple experiments.

association of rrp40 variants with the exosome, we assessed the amount and size of Myc-tagged Rrp40 and rrp40 complexes in wild-type and *doa3-1* cells grown at 37° by native-PAGE (Figure 7A). We used the *doa3-1* proteasome mutant cells to increase the amount of rrp40-W195R for comparison to wild-type Rrp40. A high amount of wild-type Rrp40 in wild-type and *doa3-1* cells migrates as a single complex of ~600 kDa on a native gel (Figure 7A). This band size is consistent with the 600 kDa size reported for the 11-subunit yeast exosome complex (Liu *et al.* 2006). In contrast, a very low amount of the rrp40-W195R variant migrating as a 600 kDa complex is detected even upon long exposure of the immunoblot (Figure 7A). The amounts of the rrp40-G8A and rrp40-S87A variants migrating as a 600 kDa complex are similar to wild-type Rrp40 (Figure 7A). Importantly, analysis of the same lysates used in the native-PAGE by denaturing SDS-PAGE shows that the level of rrp40-W195R does increase in *doa3-1* cells relative to wild-type cells (Figure 7B). The reduced amount of rrp40-W195R in the 600 kDa complex on the native gel is therefore not just due to low levels of this variant. We also find that a greater amount of the rrp40-W195R variant is present in the 600 kDa complex when it is the only copy of Rrp40 in *rrp40Δ* cells (Figure S5). To complement the native gel analysis of rrp40-W195R, we also examined wild-type and rrp40-W195R proteins in *doa3-1* cells by glycerol gradient fractionation (Figure S6). While the majority of wild-type Rrp40 is present in fractions from the middle of the gradient

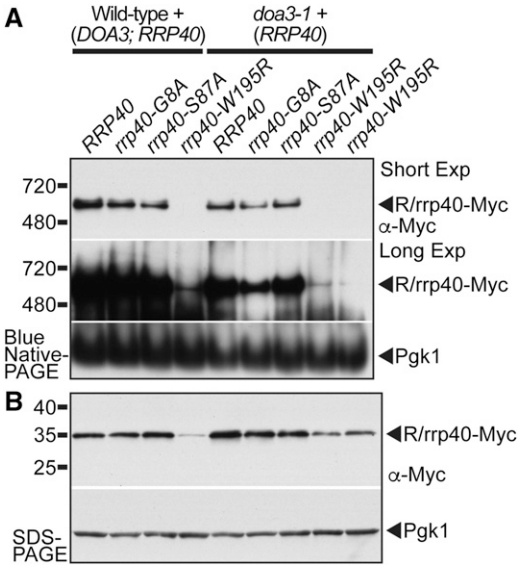

Figure 7 The rrp40-W195R variant associates less efficiently than wild-type Rrp40 with the RNA exosome complex in *S. cerevisiae* cells coexpressing wild-type Rrp40. (A) Unlike wild-type Rrp40, only a low amount of the rrp40-W195R variant in *doa3-1* cells migrates as a 600 kDa complex that is consistent with the size of the 11-subunit exosome (Liu *et al.* 2006) by native gel electrophoresis. In contrast, a similar amount of rrp40-G8A and rrp40-S87A variant compared to wild-type Rrp40 migrates as a 600 kDa complex. Lysates of wild-type and *doa3-1* temperature-sensitive proteasome mutant cells expressing Myc-tagged wild-type Rrp40 or variant rrp40 (G8A, S87A, and W195R) were grown at 37° and analyzed by BN-PAGE and immunoblotting with anti-Myc antibody to detect Myc-tagged Rrp40 proteins (R/rrp40-Myc) and anti-Pgk1 antibody to detect Pgk1 as a loading control. (B) In the same lysates analyzed by native PAGE in (A), the amount of rrp40-W195R variant in *doa3-1* cells is increased and stabilized relative to wild-type cells analyzed by denaturing SDS-PAGE. Lysates were analyzed by immunoblotting anti-Myc antibody to detect Myc-tagged Rrp40 proteins (R/rrp40-Myc), and anti-Pgk1 antibody to detect Pgk1 as a loading control.

(fractions 7–13; Figure S6A), the majority of the rrp40-W195R is present in the heaviest fraction (fraction 21; Figure S6B). These results suggest the rrp40-W195R variant associates less efficiently with the RNA exosome than wild-type Rrp40.

The mouse EXOSC3-W237R variant is expressed at reduced level when coexpressed with wild-type EXOSC3 in neuronal cells

The results presented here have employed budding yeast to assess the functional consequences of amino acid substitutions that occur in EXOSC3 in PCH1b patients. To determine whether the results obtained using budding yeast Rrp40 extend to EXOSC3 to mammalian cells, we generated substitutions in mouse EXOSC3 corresponding to PCH1b-associated substitutions and those analyzed in budding yeast Rrp40: mouse EXOSC3-G31A (human EXOSC3-G31A/yeast rrp40-G8A) and mouse EXOSC3-W237R (human EXOSC3-W238R/yeast rrp40-W195R). Wild-type and variant EXOSC3 proteins were N-terminally Myc-tagged to permit detection. We transfected plasmids that express these mouse EXOSC3 proteins into a mouse N2a neuronal cell line (Klebe and Ruddle 1969), and analyzed the steady-state levels of these Myc-tagged proteins by immunoblotting (Figure 8). To control for transfection efficiency, we employed bicistronic plasmids that coexpress GFP. Notably, the N2a cells express endogenous EXOSC3 as well as the transfected Myc-EXOSC3 proteins. The steady-state level of the mouse EXOSC3-G31A variant was partly reduced (to 55% of wild-type level), whereas the mouse EXOSC3-W237R variant level was reduced fourfold relative to wild-type mouse EXOSC3 (Figure 8). These results suggest that the mouse EXOSC3-W237R variant, corresponding to PCH1b-associated EXOSC3-W238R variant, is unstable in the presence of wild-type EXOSC3, and that mammalian cells have conserved the mechanism to discriminate between wild-type and variant EXOSC3 subunits.

Discussion

Here, we report results of the functional impact of amino acid substitutions in the *S. cerevisiae* EXOSC3 ortholog, Rrp40, corresponding to those in PCH1b-associated EXOSC3. As the human EXOSC3 protein does not substitute for the function of the essential *S. cerevisiae* Rrp40 protein (Brouwer *et al.* 2001), we generated the amino acid substitutions in Rrp40 corresponding to those present in EXOSC3 in PCH1b patients. Our study reveals that, although a number of PCH1b-associated substitutions alter evolutionarily conserved residues present in the EXOSC3/Rrp40 protein, most of these substitutions do not alter RNA exosome function to a detectable degree in the budding yeast assays employed. However, the W195R substitution in Rrp40, corresponding to W238R in EXOSC3, causes a reproducible reduction in yeast cell growth, RNA exosome function and Rrp40 protein levels. These results provide insight into possible mechanisms of RNA exosome dysfunction, and also suggest that the relative severity of such mutations can be assessed using budding yeast. Notably, PCH1b patients compound heterozygous for *EXOSC3* (W238R) and *EXOSC3* (G31A) have severe disease and do not live beyond 1 year (Wan *et al.* 2012). Moreover, no PCH1b patients homozygous for *EXOSC3* (W238R) have been reported. Given the impact of the W195R substitution on Rrp40 function, homozygosity for *EXOSC3* (W238R) could severely impair RNA exosome function, which could be incompatible with life. Genome sequencing has identified dozens of other nonsynonymous mutations in *EXOSC3* (http://www.ncbi.nlm.nih.gov/SNP/). Budding yeast could be a useful tool in the analysis of the functional impact of EXOSC3 substitutions and could provide important information for the diagnosis of PCH1b patients and/or genetic counseling of heterozygous carriers.

Most amino acid substitutions in budding yeast Rrp40 corresponding to those in PCH1b-associated EXOSC3 that we examined did not greatly alter RNA exosome function or protein levels in the assays that we employed. This result is not that surprising, given that the RNA exosome is essential for

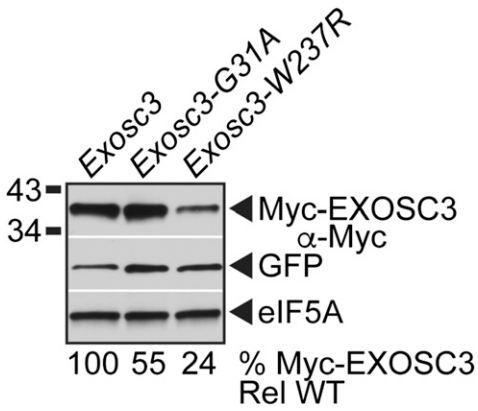

Figure 8 Variants of murine EXOSC3, corresponding to PCH1b-associated EXOSC3 variants, are expressed at reduced level in a mouse neuronal cell line. The steady-state levels of murine Myc-EXOSC3-G31A or Myc-EXOSC3-W237R variant are decreased relative to wild-type Myc-EXOSC3 in mouse N2a cells. Lysates of mouse N2a cells transfected with bicistronic vectors expressing murine Myc-EXOSC3 or Myc-EXOSC3 variant (G31A; W237R) and GFP were analyzed by immunoblotting with anti-Myc antibody to detect Myc-EXOSC3 proteins, and anti-GFP antibody to detect GFP as a transfection control. eIF5A protein was detected with anti-eIF5A antibody as a loading control. Percentage of Myc-EXOSC3 protein relative to GFP and wild-type Myc-EXOSC3 (% Myc-Exosc3 Rel WT) is shown below each lane, and was calculated as described in *Materials and Methods*. Quantitation is for the specific experiment shown, but is representative of multiple experiments.

key RNA processing steps such as rRNA maturation (Mitchell *et al.* 1996) and aberrant RNA turnover (van Hoof *et al.* 2002), but indicates that these substitutions do not cause complete loss of the Rrp40/EXOSC3 protein.

Very recently, substitutions in a second exosome cap subunit, EXOSC2, corresponding to budding yeast Rrp4, have been linked to a novel syndrome characterized by retinitis pigmentosa, hearing loss, premature aging, and intellectual disability that shows little overlap with PCH1b (Di Donato *et al.* 2016). As shown in the sequence alignment in Figure S1, one of the residues changed in these *EXOSC2* syndrome patients (EXOSC2-G30) is located in the analogous position within the N-terminal domain to the EXOSC3-G31 residue that is changed in PCH1b. Conservation from yeast to human, and between the paralogs EXOSC2 and EXOSC3, suggests that G30 and G31, respectively, are functionally important. However, we tested the function of rrp4 variants corresponding to these syndrome-associated EXOSC2 substitutions (G30V and G198D) as the sole copy of the essential Rrp4 protein, and found that they do not impair cell growth (Figure S7). Thus, like changes in Rrp40 corresponding to those in PCH1b-associated EXOSC3, substitutions in Rrp4 corresponding to those in disease-associated EXOSC2 are unlikely to cause a total loss of protein function, and most likely exert subtle effects on RNA exosome function.

A key question is how defects in the critically important and ubiquitously expressed RNA exosome complex cause tissue-specific defects. This question is particularly intriguing because mutations in the *EXOSC3* cap subunit gene affect mostly spinal motor neurons and Purkinje cells (Wan *et al.* 2012), but mutations in the *EXOSC8* core subunit gene also affect oligodendroglia cells (Boczonadi *et al.* 2014). In addition, mutations in the *EXOSC2* cap subunit gene cause a novel syndrome that is not similar to PCH disease (Di Donato *et al.* 2016). We suggest that PCH-associated substitutions in EXOSC3 or EXOSC8, and disease-related substitutions in EXOSC2, trigger subtle functional changes, perhaps impacting a specific subset of target RNAs. Such target RNAs could be different for the two PCH subtypes and the novel syndrome. For PCH1b, initial identification of the altered target RNAs in budding yeast expressing rrp40 variants by RNA-Seq would be informative. However, subsequent RNA-Seq identification of the disease-relevant target RNAs would likely need to be carried out in neuronal cells. Notably, our results suggest that merely knocking down EXOSC2, 3, or 8 expression in neuronal cells is unlikely to be as informative as examining the effect of specific disease-associated substitutions. Based on our analyses of the rrp40-W195R variant in yeast, initial mammalian studies could focus on the effects of the EXOSC3-W238R substitution variant in neuronal cells.

In contrast to the other substitutions in Rrp40 examined, corresponding to those in PCH1b-associated EXOSC3, we detected altered function for the W195R substitution in Rrp40. The presence of a bulky hydrophobic residue at this position seems to be required, as rrp40-W195R expression in *rrp40Δ* cells conferred a growth defect and an increase in the levels of exosome RNA targets at 37° when expressed as the sole copy of Rrp40, but cells expressing rrp40-W195F cells did not show a growth defect. Notably, the steady-state level and stability of the rrp40-W195R variant in *rrp40Δ* cells was reduced compared to wild-type Rrp40 at 37° (Figure 4, A and B) and at 30° (Figure 4A and Figure S4). We conclude that the rrp40-W195R substitution makes the Rrp40 protein less stable, leading to a decreased Rrp40 protein level and impaired production and/or function of the RNA exosome.

Our studies of the rrp40-W195R and -195A variants yielded a surprising finding that could have implications for understanding RNA exosome assembly and quality control (Figure 9). In *rrp40Δ* cells that express only the rrp40-W195R or –W195A variant (Figure 9B), the steady-state level of the rrp40 variant is partly reduced (63–65%) compared to wild-type Rrp40 at 30° (Figure 4A). However, in cells that express both wild-type Rrp40 and rrp40-W195R or –W195A (Figure 9C), the steady-state level of the rrp40 variant is greatly decreased (24–30%) relative to wild-type Rrp40 at 30° (Figure 5A). In addition, the stability of the rrp40-W195R variant in cells coexpressing wild-type Rrp40 is greatly decreased ($t_{1/2}$ ~6 min) compared to cells that express only rrp40-W195R ($t_{1/2}$ ~116 min) at 30° (Figure 6B and Figure S4). This finding suggests a model (Figure 9C) where cells assemble functional RNA exosome complex by distinguishing between wild-type Rrp40 and rrp40 variant. In support, we

find that the rrp40-W195R variant does not associate as efficiently with the exosome complex in cells coexpressing wild-type Rrp40 compared to cells that express only rrp40-W195R (Figure 7 and Figure S6).

Several possible mechanisms for exosome assembly could explain how cells show preference for a wild-type exosome subunit as compared to a variant subunit. Although exosome assembly factors have not yet been identified, there could be chaperones that help to ensure assembly of an optimal exosome complex. Like the proteasome, these chaperones could control the assembly of specific exosome subcomplexes or regulate the order in which specific exosome subunits or subcomplexes associate (Tomko and Hochstrasser 2013). In such a scenario, the rate of assembly of the variant subunit into the RNA exosome might be decreased relative to assembly of a wild-type subunit (Figure 9C). An alternative possibility is that assembly of Rrp40, and possibly other subunits, into the RNA exosome could be reversible at a significant rate (Figure 9C). The defects in interactions with other RNA exosome subunits caused by PCH1b-associated substitutions could increase the rate of disassembly from the complex. Thus, in the presence of wild-type Rrp40, the variant rrp40 subunit could be replaced and subsequently degraded. Further studies will be required to understand how the RNA exosome can apparently discriminate between wild-type and variant subunits.

Very little is known about RNA exosome assembly and quality control. However, a previous study of the *Trypanosoma brucei* RNA exosome subunits, *Tb*RRP4 and *Tb*RRP45, showed that high level expression of tagged *Tb*RRP4 or *Tb*RRP45 led to proteasome-dependent turnover of the corresponding endogenous exosome subunit (Estevez *et al.* 2003). Based on this latter study, and other previous work showing that neither *Tb*RRP4 nor *Tb*RRP45 was detected independent of fractions containing the RNA exosome complex in glycerol density gradient analysis (Estevez *et al.* 2001), these authors proposed that, when these subunits are not incorporated into the RNA exosome, they are subject to rapid degradation. Another finding consistent with altered RNA exosome subunit stoichiometry leading to subunit turnover comes from the recent study of *EXOSC8* mutations in PCH1c patients (Boczonadi *et al.* 2014). This latter study reported that *EXOSC8* mutations (or *EXOSC8* knockdown) that reduced the steady-state level of EXOSC8 protein led to a concomitant decrease in the level of EXOSC3 protein (Boczonadi *et al.* 2014). Consistent with these observations on the *T. brucei* and human RNA exosome, our results in yeast and mammalian cells showing that rrp40/EXOSC3 variant levels are reduced in the presence of wild-type subunit suggest that a conserved mechanism exists to ensure formation, and/or maintenance, of optimal RNA exosome complex.

In summary, the work presented here provides a rapid screening approach that exploits budding yeast to identify the most functionally impaired amino acid changes linked to PCH1b disease. In addition, our analyses of rrp40 variants provide insight into a possible mechanism for RNA exosome assembly and quality control that could be impacted by the PCH1b-associated substitutions.

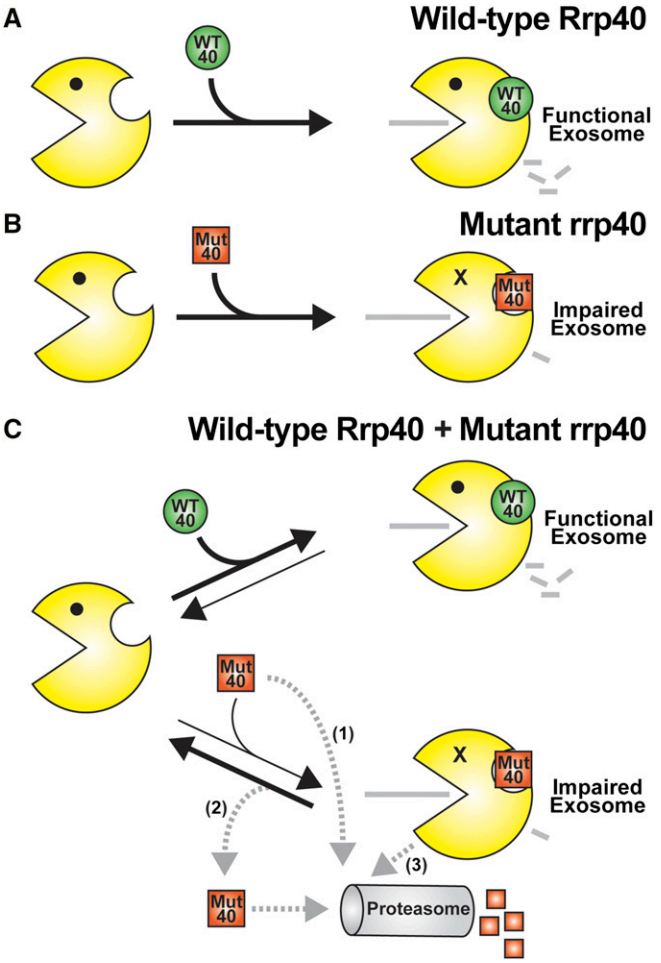

Figure 9 Model for exosome assembly and function. (A) When cells express wild-type Rrp40 (WT 40) as the only copy of Rrp40, the exosome assembles properly to produce a fully functional exosome. (B) When cells express variant rrp40-W195R (Mut 40) as the only copy of Rrp40, the exosome shows impaired function as evidenced by a modest decrease in cell growth, altered levels of exosome target transcripts, and subunit instability. (C) When cells express both wild-type Rrp40 (WT 40) and variant rrp40-W195R (Mut 40), the rrp40-W195R is highly unstable and degraded rapidly in a proteasome-dependent manner. As indicated by the black arrows depicting RNA exosome complex assembly and disassembly, the rrp40-W195R protein (Mut 40) could be assembled into the RNA exosome less efficiently than the wild-type Rrp40 (WT 40), or the exosome complex assembled with rrp40-W195R (Mut 40) could be disassembled more rapidly than the exosome containing wild-type Rrp40. Importantly, reduced association of rrp40-W195R with the exosome in cells expressing wild-type Rrp40 is supported by native gel and glycerol gradient analysis. Several possible routes for degradation of rrp40-W195R (Mut 40) exist (gray dashed arrows): (1) Mut 40 subunit could be degraded directly without ever being incorporated into the RNA exosome; (2) Mut 40 subunit that results from disassembly of the exosome complex could be targeted for degradation; or (3) the entire RNA exosome assembled with Mut 40 could be targeted for degradation. Further studies will be required to distinguish between these possible mechanisms for rapid, proteasome-mediated turnover of the rrp40 variant.

Acknowledgments

We thank members of the Corbett and van Hoof laboratories for critical discussions. This work was supported by National Institutes of Health (NIH) R01 grants (GM058728) to A.H. C. and (GM099790) to A.v.H. S.B. was supported by NIH R25 GM099644. B.A. was supported by the Howard Hughes Medical Institute Science Education Program award #52006923 to Emory University. J.C.V. was supported by a summer research stipend from The University of Texas Graduate School of Biomedical Sciences at Houston. Any opinions, findings, and conclusions or recommendations expressed in this material are those of the author(s) and do not necessarily reflect the views of the NIH, Howard Hughes Medical Institute, Emory University, or The University of Texas.

Literature Cited

Adams, A., D. E. Gottschling, C. A. Kaiser, and T. Stearns, 1997 *Methods in Yeast Genetics*. Cold Spring Harbor Laboratory Press, Cold Spring Harbor, NY.

Agamy, O., B. Ben Zeev, D. Lev, B. Marcus, D. Fine *et al.*, 2010 Mutations disrupting selenocysteine formation cause progressive cerebello-cerebral atrophy. Am. J. Hum. Genet. 87: 538–544.

Akizu, N., V. Cantagrel, J. Schroth, N. Cai, K. Vaux *et al.*, 2013 AMPD2 regulates GTP synthesis and is mutated in a potentially treatable neurodegenerative brainstem disorder. Cell 154: 505–517.

Allmang, C., E. Petfalski, A. Podtelejnikov, M. Mann, D. Tollervey *et al.*, 1999 The yeast exosome and human PM-Scl are related complexes of 3′ → 5′ exonucleases. Genes Dev. 13: 2148–2158.

Belle, A., A. Tanay, L. Bitincka, R. Shamir, and E. K. O'Shea, 2006 Quantification of protein half-lives in the budding yeast proteome. Proc. Natl. Acad. Sci. USA 103: 13004–13009.

Biancheri, R., D. Cassandrini, F. Pinto, R. Trovato, M. Di Rocco *et al.*, 2013 EXOSC3 mutations in isolated cerebellar hypoplasia and spinal anterior horn involvement. J. Neurol. 260: 1866–1870.

Boczonadi, V., J. S. Muller, A. Pyle, J. Munkley, T. Dor *et al.*, 2014 EXOSC8 mutations alter mRNA metabolism and cause hypomyelination with spinal muscular atrophy and cerebellar hypoplasia. Nat. Commun. 5: 4287.

Bonneau, F., J. Basquin, J. Ebert, E. Lorentzen, and E. Conti, 2009 The yeast exosome functions as a macromolecular cage to channel RNA substrates for degradation. Cell 139: 547–559.

Brouwer, R., C. Allmang, R. Raijmakers, Y. van Aarssen, W. V. Egberts *et al.*, 2001 Three novel components of the human exosome. J. Biol. Chem. 276: 6177–6184.

Brown, J. T., X. Bai, and A. W. Johnson, 2000 The yeast antiviral proteins Ski2p, Ski3p, and Ski8p exist as a complex in vivo. RNA 6: 449–457.

Budde, B. S., Y. Namavar, P. G. Barth, B. T. Poll-The, G. Nurnberg *et al.*, 2008 tRNA splicing endonuclease mutations cause pontocerebellar hypoplasia. Nat. Genet. 40: 1113–1118.

Butler, J. S., and P. Mitchell, 2010 Rrp6, Rrp47 and cofactors of the nuclear exosome. Adv. Exp. Med. Biol. 702: 91–104.

Buttner, K., K. Wenig, and K. P. Hopfner, 2005 Structural framework for the mechanism of archaeal exosomes in RNA processing. Mol. Cell 20: 461–471.

Chapman, M. A., M. S. Lawrence, J. J. Keats, K. Cibulskis, C. Sougnez *et al.*, 2011 Initial genome sequencing and analysis of multiple myeloma. Nature 471: 467–472.

Chen, P., and M. Hochstrasser, 1996 Autocatalytic subunit processing couples active site formation in the 20S proteasome to completion of assembly. Cell 86: 961–972.

Di Donato, N., T. Neuhann, A. K. Kahlert, B. Klink, K. Hackmann *et al.*, 2016 Mutations in EXOSC2 are associated with a novel syndrome characterised by retinitis pigmentosa, progressive hearing loss, premature ageing, short stature, mild intellectual disability and distinctive gestalt. J. Med. Genet. 53: 419–425.

Dziembowski, A., E. Lorentzen, E. Conti, and B. Seraphin, 2007 A single subunit, Dis3, is essentially responsible for yeast exosome core activity. Nat. Struct. Mol. Biol. 14: 15–22.

Edvardson, S., A. Shaag, O. Kolesnikova, J. M. Gomori, I. Tarassov *et al.*, 2007 Deleterious mutation in the mitochondrial arginyl-transfer RNA synthetase gene is associated with pontocerebellar hypoplasia. Am. J. Hum. Genet. 81: 857–862.

Eggens, V. R., P. G. Barth, J. M. Niermeijer, J. N. Berg, N. Darin *et al.*, 2014 EXOSC3 mutations in pontocerebellar hypoplasia type 1: novel mutations and genotype-phenotype correlations. Orphanet J. Rare Dis. 9: 23.

Estevez, A. M., T. Kempf, and C. Clayton, 2001 The exosome of *Trypanosoma brucei*. EMBO J. 20: 3831–3839.

Estevez, A. M., B. Lehner, C. M. Sanderson, T. Ruppert, and C. Clayton, 2003 The roles of intersubunit interactions in exosome stability. J. Biol. Chem. 278: 34943–34951.

Fabre, A., B. Charroux, C. Martinez-Vinson, B. Roquelaure, E. Odul *et al.*, 2012 SKIV2L mutations cause syndromic diarrhea, or trichohepatoenteric syndrome. Am. J. Hum. Genet. 90: 689–692.

Fabre, A., A. Breton, M. E. Coste, V. Colomb, B. Dubern *et al.*, 2013 Syndromic (phenotypic) diarrhoea of infancy/tricho-hepato-enteric syndrome. Arch. Dis. Child. 99: 35–38

Fang, F., J. Hoskins, and J. S. Butler, 2004 5-fluorouracil enhances exosome-dependent accumulation of polyadenylated rRNAs. Mol. Cell. Biol. 24: 10766–10776.

Han, J., and A. van Hoof, 2016 The RNA exosome channeling and direct access conformations have distinct in vivo functions. Cell Reports 16: 3348–3358.

Hanada, T., S. Weitzer, B. Mair, C. Bernreuther, B. J. Wainger *et al.*, 2013 CLP1 links tRNA metabolism to progressive motor-neuron loss. Nature 495: 474–480.

Hartley, J. L., N. C. Zachos, B. Dawood, M. Donowitz, J. Forman *et al.*, 2010 Mutations in TTC37 cause trichohepatoenteric syndrome (phenotypic diarrhea of infancy). Gastroenterology 138: 2388–2398.e2.

Jacobs Anderson, J. S., and R. Parker, 1998 The 3′ to 5′ degradation of yeast mRNAs is a general mechanism for mRNA turnover that requires the SKI2 DEVH box protein and 3′ to 5′ exonucleases of the exosome complex. EMBO J. 17: 1497–1506.

Kadaba, S., A. Krueger, T. Trice, A. M. Krecic, A. G. Hinnebusch *et al.*, 2004 Nuclear surveillance and degradation of hypomodified initiator $tRNA^{Met}$ in *S. cerevisiae*. Genes Dev. 18: 1227–1240.

Klebe, R. J., and F. H. Ruddle, 1969 Neuroblastoma: cell culture analysis of a differentiating stem cell system. J. Cell Biol. 43: 69a.

Kowalinski, E., A. Kogel, J. Ebert, P. Reichelt, E. Stegmann *et al.*, 2016 Structure of a cytoplasmic 11-subunit RNA exosome complex. Mol. Cell 63: 125–134.

LaCava, J., J. Houseley, C. Saveanu, E. Petfalski, E. Thompson *et al.*, 2005 RNA degradation by the exosome is promoted by a nuclear polyadenylation complex. Cell 121: 713–724.

Lebreton, A., R. Tomecki, A. Dziembowski, and B. Seraphin, 2008 Endonucleolytic RNA cleavage by a eukaryotic exosome. Nature 456: 993–996.

Li, X., A. R. Kusmierczyk, P. Wong, A. Emili, and M. Hochstrasser, 2007 Beta-subunit appendages promote 20S proteasome assembly by overcoming an Ump1-dependent checkpoint. EMBO J. 26: 2339–2349.

Liu, J. J., M. A. Bratkowski, X. Liu, C. Y. Niu, A. Ke *et al.*, 2014 Visualization of distinct substrate-recruitment pathways in the yeast exosome by EM. Nat. Struct. Mol. Biol. 21: 95–102.

Liu, Q., J. C. Greimann, and C. D. Lima, 2006 Reconstitution, activities, and structure of the eukaryotic RNA exosome. Cell 127: 1223–1237.

Livak, K. J., and T. D. Schmittgen, 2001 Analysis of relative gene expression data using real-time quantitative PCR and the 2(-Delta C(T)). Method. Methods 25: 402–408.

Lorentzen, E., A. Dziembowski, D. Lindner, B. Seraphin, and E. Conti, 2007 RNA channelling by the archaeal exosome. EMBO Rep. 8: 470–476.

Lubas, M., M. S. Christensen, M. S. Kristiansen, M. Domanski, L. G. Falkenby *et al.*, 2011 Interaction profiling identifies the human nuclear exosome targeting complex. Mol. Cell 43: 624–637.

Lubas, M., P. R. Andersen, A. Schein, A. Dziembowski, G. Kudla *et al.*, 2015 The human nuclear exosome targeting complex is loaded onto newly synthesized RNA to direct early ribonucleolysis. Cell Reports 10: 178–192.

Lum, P. Y., C. D. Armour, S. B. Stepaniants, G. Cavet, M. K. Wolf *et al.*, 2004 Discovering modes of action for therapeutic compounds using a genome-wide screen of yeast heterozygotes. Cell 116: 121–137.

Makino, D. L., M. Baumgartner, and E. Conti, 2013 Crystal structure of an RNA-bound 11-subunit eukaryotic exosome complex. Nature 495: 70–75.

Malet, H., M. Topf, D. K. Clare, J. Ebert, F. Bonneau *et al.*, 2010 RNA channelling by the eukaryotic exosome. EMBO Rep. 11: 936–942.

Mitchell, P., E. Petfalski, and D. Tollervey, 1996 The 3′ end of yeast 5.8S rRNA is generated by an exonuclease processing mechanism. Genes Dev. 10: 502–513.

Mitchell, P., E. Petfalski, A. Shevchenko, M. Mann, and D. Tollervey, 1997 The exosome: a conserved eukaryotic RNA processing complex containing multiple 3′→5′ exoribonucleases. Cell 91: 457–466.

Mochida, G. H., V. S. Ganesh, M. I. de Michelena, H. Dias, K. D. Atabay *et al.*, 2012 CHMP1A encodes an essential regulator of BMI1–INK4A in cerebellar development. Nat. Genet. 44: 1260–1264.

Namavar, Y., D. Chitayat, P. G. Barth, F. van Ruissen, M. B. de Wissel *et al.*, 2011 TSEN54 mutations cause pontocerebellar hypoplasia type 5. Eur. J. Hum. Genet. 19: 724–726.

Renbaum, P., E. Kellerman, R. Jaron, D. Geiger, R. Segel *et al.*, 2009 Spinal muscular atrophy with pontocerebellar hypoplasia is caused by a mutation in the VRK1 gene. Am. J. Hum. Genet. 85: 281–289.

Robinson, S. R., A. W. Oliver, T. J. Chevassut, and S. F. Newbury, 2015 The 3′ to 5′ exoribonuclease DIS3: from structure and mechanisms to biological functions and role in human disease. Biomolecules 5: 1515–1539.

Rudnik-Schoneborn, S., J. Senderek, J. C. Jen, G. Houge, P. Seeman *et al.*, 2013 Pontocerebellar hypoplasia type 1: clinical spectrum and relevance of EXOSC3 mutations. Neurology 80: 438–446.

Sambrook, J., E. F. Fritsch, and T. Maniatis, 1989 *Molecular Cloning: A Laboratory Manual*. Cold Spring Harbor Laboratory Press, Cold Spring Harbor, NY.

Schaeffer, D., S. Meaux, A. Clark, and A. van Hoof, 2008 Determining *in vivo* activity of the yeast cytoplasmic exosome. Methods Enzymol. 448: 227–239.

Schaeffer, D., B. Tsanova, A. Barbas, F. P. Reis, E. G. Dastidar *et al.*, 2009 The exosome contains domains with specific endoribonuclease, exoribonuclease and cytoplasmic mRNA decay activities. Nat. Struct. Mol. Biol. 16: 56–62.

Schaeffer, D., A. Clark, A. A. Klauer, B. Tsanova, and A. van Hoof, 2010 Functions of the cytoplasmic exosome, in *RNA Exosome*, edited by T. H. Jensen. Landes Bioscience, New York.

Schaffer, A. E., V. R. Eggens, A. O. Caglayan, M. S. Reuter, E. Scott *et al.*, 2014 CLP1 founder mutation links tRNA splicing and maturation to cerebellar development and neurodegeneration. Cell 157: 651–663.

Schilders, G., R. Raijmakers, J. M. Raats, and G. J. Pruijn, 2005 MPP6 is an exosome-associated RNA-binding protein involved in 5.8S rRNA maturation. Nucleic Acids Res. 33: 6795–6804.

Schilders, G., E. van Dijk, and G. J. Pruijn, 2007 C1D and hMtr4p associate with the human exosome subunit PM/Scl-100 and are involved in pre-rRNA processing. Nucleic Acids Res. 35: 2564–2572.

Schneider, C., and D. Tollervey, 2013 Threading the barrel of the RNA exosome. Trends Biochem. Sci. 38: 485–493.

Schwabova, J., D. S. Brozkova, B. Petrak, M. Mojzisova, K. Pavlickova *et al.*, 2013 Homozygous EXOSC3 mutation c.92G→C, p.G31A is a founder mutation causing severe pontocerebellar hypoplasia type 1 among the Czech Roma. J. Neurogenet. 27: 163–169.

Shcherbik, N., M. Wang, Y. R. Lapik, L. Srivastava, and D. G. Pestov, 2010 Polyadenylation and degradation of incomplete RNA polymerase I transcripts in mammalian cells. EMBO Rep. 11: 106–111.

Sikorski, R. S., and P. Hieter, 1989 A system of shuttle vectors and yeast host strains designed for efficient manipulation of DNA in *Saccharomyces cerevisiae*. Genetics 122: 19–27.

Sloan, K. E., C. Schneider, and N. J. Watkins, 2012 Comparison of the yeast and human nuclear exosome complexes. Biochem. Soc. Trans. 40: 850–855.

Staals, R. H., A. W. Bronkhorst, G. Schilders, S. Slomovic, G. Schuster *et al.*, 2010 Dis3-like 1: a novel exoribonuclease associated with the human exosome. EMBO J. 29: 2358–2367.

Tomecki, R., M. S. Kristiansen, S. Lykke-Andersen, A. Chlebowski, K. M. Larsen *et al.*, 2010 The human core exosome interacts with differentially localized processive RNases: hDIS3 and hDIS3L. EMBO J. 29: 2342–2357.

Tomecki, R., K. Drazkowska, I. Kucinski, K. Stodus, R. J. Szczesny *et al.*, 2013 Multiple myeloma-associated hDIS3 mutations cause perturbations in cellular RNA metabolism and suggest hDIS3 PIN domain as a potential drug target. Nucleic Acids Res. 42: 1270–1290.

Tomko, Jr., R. J., and M. Hochstrasser, 2013 Molecular architecture and assembly of the eukaryotic proteasome. Annu. Rev. Biochem. 82: 415–445.

van Hoof, A., R. R. Staples, R. E. Baker, and R. Parker, 2000 Function of the ski4p (Csl4p) and Ski7p proteins in 3′-to-5′ degradation of mRNA. Mol. Cell. Biol. 20: 8230–8243.

van Hoof, A., P. A. Frischmeyer, H. C. Dietz, and R. Parker, 2002 Exosome-mediated recognition and degradation of mRNAs lacking a termination codon. Science 295: 2262–2264.

Vasiljeva, L., and S. Buratowski, 2006 Nrd1 interacts with the nuclear exosome for 3′ processing of RNA polymerase II transcripts. Mol. Cell 21: 239–248.

Wan, J., M. Yourshaw, H. Mamsa, S. Rudnik-Schoneborn, M. P. Menezes *et al.*, 2012 Mutations in the RNA exosome component gene EXOSC3 cause pontocerebellar hypoplasia and spinal motor neuron degeneration. Nat. Genet. 44: 704–708.

Wasmuth, E. V., and C. D. Lima, 2012 Structure and activities of the eukaryotic RNA exosome. Enzymes 31: 53–75.

Wasmuth, E. V., K. Januszyk, and C. D. Lima, 2014 Structure of an Rrp6-RNA exosome complex bound to poly(A) RNA. Nature 511: 435–439.

Wichtowska, D., T. W. Turowski, and M. Boguta, 2013 An interplay between transcription, processing, and degradation determines tRNA levels in yeast. Wiley Interdiscip. Rev. RNA 4: 709–722.

Wittig, I., H. P. Braun, and H. Schagger, 2006 Blue native PAGE. Nat. Protoc. 1: 418–428.

Communicating editor: M. Hampsey

SUPPORTING INFORMATION

Table S1 - Yeast Strains and Plasmids

Strain/Plasmid	Description	Source
*rrp40*Δ (yAV1107)	*MATa his3*Δ*1 leu2*Δ*0 ura3*Δ*0 rrp40*Δ*::NEO* [*RRP40,URA3*]	(SCHAEFFER *et al.* 2009)
*ski7*Δ (yAV571)	*MATa, leu2*Δ*0, ura3*Δ*0, his3*Δ*1, met15*Δ*0, ski7*Δ*::NEO*	(VAN HOOF *et al.* 2000)
doa3-1 (MHY3646)	*MAT*α *his3-*Δ*200 leu2-3,112 ura3-52 lys2-801 trp1-1 doa3-*Δ*1::HIS3* [*prg1-3*, *TRP1*]	(LI *et al.* 2007)
Wild-type (MHY501)	*MAT*α *his3-*Δ*200 leu2-3,112 ura3-52 lys2-801 trp1-1*	(CHEN AND HOCHSTRASSER 1996)
RRP40-TAP	*MATa ura3*Δ *leu2*Δ *his3*Δ *RRP40-TAP:HIS3MX6* (BY4741)	Dharmacon
*rrp4*Δ (yAV1104)	*MATa his3*Δ*1 leu2*Δ*0 ura3*Δ*0 lys2*Δ*0 rrp4*Δ*::NEO* [*RRP4,URA3*]	(SCHAEFFER *et al.* 2009)
Wild-type (BY4741)	*MATa leu2*Δ *ura3*Δ *his3*Δ *TRP1 met15*Δ	Research Genetics
pRS315	*CEN6, LEU2, amp*^{R}	(SIKORSKI AND HIETER 1989)
pRS415	*CEN6, LEU2, amp*^{R}	(SIKORSKI AND HIETER 1989)
pAC3016	*RRP40-2xMyc, 2μ, URA3, amp*^{R}	This Study
pAC3161	*RRP40-2xMyc* in pRS315*, CEN6, LEU2, amp*^{R}	This Study
pAC3162	*rrp40-G8A-2xMyc* in pRS315*, CEN6, LEU2, amp*^{R}	This Study
pAC3163	*rrp40-W195A-2xMyc* in pRS315, *CEN6, LEU2, amp*^{R}	This Study
pAC3257	*rrp40-S87A-2xMyc* in pRS315, *CEN6, LEU2, amp*^{R}	This Study
pAC3259	*rrp40-W195R-2xMyc* in pRS315, *CEN6, LEU2, amp*^{R}	This Study
pAC3286	*rrp40-W195F-2xMyc* in pRS315*, CEN6, LEU2, amp*^{R}	This Study
pIGneo	CMV-IRES, *EGFP*, *neo*, *amp*^{R}	Addgene
pAC3417	*2xMyc-Exosc3* in pIGneo*, amp*^{R}	This Study
pAC3418	*2xMyc-Exosc3*^{G31A} in pIGneo*, amp*^{R}	This Study
pAC3420	*2xMyc-Exosc3*^{W237R} in pIGneo*, amp*^{R}	This Study
pAV188	*his3-nonstop* in pRS416, *CEN6, URA3, amp*^{R}	(VAN HOOF *et al.* 2002)
pAV991	*RRP4* in pRS415, *CEN6, LEU2, amp*^{R}	This Study
pAV1181	*rrp4-G58V* in pRS415, *CEN6, LEU2, amp*^{R}	This Study
pAV1183	*rrp4-G226D* in pRS415, *CEN6, LEU2, amp*^{R}	This Study

Table S2 - DNA Oligonucleotides for Quantitative RT-PCR

Description	Sequence (5'-3')	Name
NEL025c CUT Fwd	CGCAGAGTTCTTACCAAACG	AC5726
NEL025c CUT Rev	GCAAAGATCTGTATGAAAGG	AC5727
U4 snRNA Fwd	AAAGAATGAATATCGGTAATG	AC5722
U4 snRNA Rev	ATCCTTATGCACGGGAAATACG	AC5723
ITS-2 rRNA Fwd	AGATTAGCCGCAGTTGG	AC5724
ITS-2 rRNA Rev	AGCGTCATTTCCTTCTCA	AC5725
ALG10 mRNA Fwd	CACGGATAGTGGCTTTGGTGAACAATTAC	AC5067
ALG10 mRNA Rev	TATGATTATCTGGCAGCAGGAAAGAACTTGGG	AC5068

```
                                                                 EXOSC3-G31
HsEXOSC3     1 MAEPA---------------------------SVAAESLAGSRARAARTVLGQVVLPGEE
MmEXOSC3     1 MAEVL---------------------------SAGPESVAGCRARAVHKVLNQVVLPGEE
DrRrp40      1 --------------------------------------MDSSVHTSLLERIGDVVLPGDL
DmRrp40      1 -----------------------------------------------MSATSTIVMPGER
CeRrp40      1 ---------------------------------------------------MTVYLPGDV
ScRrp40      1 --------------------------------------------------MSTFIFPGDS
SpRrp40      1 ------------------------------------------MAEVEEKGLLSYYFPGER
CnRrp40      1 --------------------------------------------------MPTLILPGET
AtRrp40      1 --------------------------------------MAAKVSVSPTSLLNQIVVPGDV
OsRrp40      1 ---------------------------------------MESRKPPPSALVDNHVVPGDV
SsRrp4       1 --------------------------------------MNMSQSQKIVLQPRSIVVPGEL
HsEXOSC2     1 -------------MAMEM---------------RLPVARKPLSERLGRDTKKHLVVPGDT
ScRrp4       1 MSEVITITKRNGAFQNSSNLSYNNTGISDDENDEEDIYMHDVNSASKSESDSQIVTPGEL
consensus    1                                                      vvlPGe
                                                                 EXOSC2-G30

HsEXOSC3    34 LLLPEQEDAEGPGGAVERPLSLNARACSRVRVVCGPGLRRCGDR----------------
MmEXOSC3    34 LVLPDHEDVDGLGGAGEQPLRLNAGARPRLRVVCGPGLRRCGDR----------------
DrRrp40     23 LFSFSPPE-------------AGDANPKADRLICGPGLRRSGAE----------------
DmRrp40     14 IAA-------------------IEELAKSKRVILGPGLRRLDDT----------------
CeRrp40     10 INEPSS----------------------SDSSIIGYGISVRGQT----------------
ScRrp40     11 FPVDP-----------------------TTPVKLGPGIYCDPNTQE--------------
SpRrp40     19 IPDSIIS--------------------QDGSIRLGPGLVFQKKDRE------------EE
CnRrp40     11 VPIPS----------------------TSKAVVLGPGISQSTPTLQASSSTASGSSSAQG
AtRrp40     23 VLDLSNM--------------------NNQTIKLGSGLLQDNDA----------------
OsRrp40     22 VLDLAEM--------------------TNQTIKLGAGLRQDCDT----------------
SsRrp4      23 LAEGEF------------------------QIPWSPYILKINSK----------------
HsEXOSC2    33 ITTDTG-------------------------FMRGHGTYMGEEK----------------
ScRrp4      61 VTDDPI-------------------------WMRGHGTYFLDNM----------------
consensus   61 l                              v  g gl

                                                               EXOSC3-D132
HsEXOSC3    78 LLVTKCGRLRHKEPGSGSGGGVYWVDSQQKRYVPVKGDHVIGIVTAKSGDIFKVDVGGS-
MmEXOSC3    78 LLVTKCGRLRHKEPS-GGGGGVYWVDSQQKRYVPVKGDHVIGIVIAKSGDIFKVDVGGS-
DrRrp40     54 IRVCRAGVLKHKQPN------MYWVNCQQRRYVPAKGESVIGIVTAKSGDVFKVDVGGS-
DmRrp40     39 VVASKAGPLRHKEPG------TFWVDNYQRRYIPARGDLILGIVRAKAGDLYRVDIGAT-
CeRrp40     32 RIATQPGAFH-------NDDGKVWLNVHSKRYIPQEGDRVIAIVTSKTGDFFRLDIGTA-
ScRrp40     34 IRPVNTGVLHVSAKG-KSGVQTAYIDYSSKRYIPSVNDFVIGVIIGTFSDSYKVSLQNFS
SpRrp40     47 IVVSKAGRLH-Q-----TGKNAMLIDSRTKRYIPATNDQVIGQIISRFAEGYRVDIGSA-
CnRrp40     49 YIATRLGMLH-SGKG-KERSQKLWIEGNSKRYIPAQKDIVLGIIIARHADGYRVDLGSS-
AtRrp40     47 ISAMRAGKLSYSKPN------KYWLESSHKRYIPRPDDHVLGIVVDSRADNFWVDIKGP-
OsRrp40     46 IQATSAGRLRLSKPS------KYWVESSQKRYIPSVEDTVLGVVVDTKPDNFLVDIKGP-
SsRrp4      43 YYSTVVGLFDVKDTQ------FEVIPLEGSFYYPKINDIVIGLVEDVEIYGWVVDIKAP-
HsEXOSC2    52 LIASVAGSVERVN-------KLICVKALKTRYIGEVGDIVVGRITEVQQKRWKVETNSR-
ScRrp4      80 TYSSVAGTVSRVN-------RLLSVIPLKGRYAPETGDHVVGRIAEVGNKRWKVDIGGK-
consensus  121    t  G l               v     krYvp   d vigiv     d fkvdv
```

```
                EXOSC3-A139
HsEXOSC3    137 EPA--SLSYLSFEGAT---------KRNRPNVQVGDLIYGQFVVANKDMEPEMVCIDS-C
MmEXOSC3    136 EPA--SLSYLAFEGAT---------KRNRPNVQVGDLIYGQCVVANKDMEPEMVCIDS-C
DrRrp40     107 EQA--SLSYLAFEGAT---------KRNRPNVQVGDLVFGQFTIANKDMEPELVCIDS-C
DmRrp40      92 DTA--SISYLAFEAAS---------KKNRPDLIPGDLIYARVLNASADIEPELVCVNS-V
CeRrp40      84 EYA--MINFTNFEGAT---------KRNRPNLKTGDIIYATVFDTTPRTEAELTCVDD-E
ScRrp40      93 SSV--SLSYMAFPNAS---------KKNRPTLQVGDLVYARVCTAEKELEAEIECFDSTT
SpRrp40     100 HIA--QLNALAFENVT---------RKSRPNLNVGSLVYARVSLADRDMEPELECFDATT
CnRrp40     106 QMA--QLDALAFEGAT---------KRSKPNLKVGTLVFARVMSASRDMEPELECFDPNT
AtRrp40     100 QLA--LLPVLAFEGGT---------RRNIPKFEVGTLLYLRVVKTNIGMNPELSCTEA-S
OsRrp40      99 NLA--FLPVLAFEGGT---------RRNIPKFEIGTLIYARVVKANSIMNPELSCMDA-T
SsRrp4       96 YKA--YLPASNLLGRSINV-----GEDLRRYLDVGDYVIARIENFDRSIDPVLSVKGKD-
HsEXOSC2    104 LDSVLLLSSMNLPGGELRRRSAEDELAMRGFLQEGDLISAEVQAVFSDGAVSL------H
ScRrp4      132 QHAVLMLGSVNLPGGILRRKSESDELQMRSFLKEGDLLNAEVQSLFQDGSASL------H
consensus   181   a   l  l f gat         kr rp v  G liyg v      m  el c

                                                                EXOSC3-W238
HsEXOSC3    185 GRANGMGVIGQDGLLFK-VTLGLIRKLLA-PDCEIIQEVGKLYP--LEIVFGMNGRIWVK
MmEXOSC3    184 GRANGMGVIGQDGLLFK-VTLGLIRKLLA-PDCEIVQELGKLYP--LEIVFGMNGRIWVK
DrRrp40     155 GRANGMGVFGGDGLLFK-VSLGLVRRLLA-PQSDLVSDLEKMFP--CEMVVGMNGRVWVK
DmRrp40     140 GKSGKLGVL-TDGFFFK-CSLNLGRMLLR-ENCPVLAALTRELP--YEIAVGVNGRIWLK
CeRrp40     132 KRARGMGQL-NGGFMFK-VSLNHCRRLIN-PSCKILQTVGKFFK--FEITVGMNGRIWIS
ScRrp40     142 GRDAGFGIL-EDGMIID-VNLNFARQLLFNNDFPLLKVLAAHTK--FEVAIGLNGKIWVK
SpRrp40     149 GKAAGYGEL-KNGYMITGLSLSHCRKLILPKN-TLLQTLGSYIP--FEIAVGMNGRVWVN
CnRrp40     155 GKSDGFGEL-KGGVMVN-ATLQLCRRLLDRNH-IVLPTIASIFP--FEIAIGLNGRVWMK
AtRrp40     148 GKAALFGPL-RDGFMFE-TSTGLSRMLLNSPTRPVIEALGKKLS--FEIAVGLNGRVWVN
OsRrp40     147 GKAAEFGQL-KDGYMFD-TSTGLSRMLLSSPTCPILEALGKKLS--FEIAVGLNGRVWVN
SsRrp4      148 -----LGRV-SNGIVIDIMPVK-VPRVIG-KNKSMYETLTSKSG--CSIFVANNGRIWAT
HsEXOSC2    158 TRSLKYGKL-GQGVLVQ-VSPSLVKRQKT---------HFHDLPCGASVILGNNGFIWIY
ScRrp4      186 TRSLKYGKL-RNGMFCQ-VPSSLIVRAKN---------HTHNLPGNITVVLGVNGYIWLR
consensus   241  r    G i   G l    t    r ll      ii  v        ei vgmNGriWv
                                                    EXOSC2-G198

HsEXOSC3    241 AKTIQQTLILANILEACEHMTSDQRK---------Q------IFSRLAE----S------
MmEXOSC3    240 AKTIQQTLILANVLEACEHMTTEQRK---------Q------IFARLAE----S------
DrRrp40     211 ARTVQHTLILSNLLEACENMSTAQRH---------T------LFRRVAD----GGI----
DmRrp40     195 AHSLKETVALANAISALEQSGCAEID---------K------ICGNLGD----FLQA---
CeRrp40     187 ASTSDDIIKIHDIINKSEFITDEDEL---------ITLVQNNYTRSVSD-----------
ScRrp40     198 CEELSNTLACYRTIMECCQKNDTAAF---------KDIAKRQFKEILTV----KEE----
SpRrp40     205 SENLSTTVLICTAIRNCEFMSDEEQI---------KYC-KDLIKKL--------------
CnRrp40     210 AETVGETLAMKRLIESVDDHIIPVEE---------KAI-KEKLREYLS------------
AtRrp40     204 ATAPRIVIIVANAIMNSESLSGTQQR---------I--MVEKLLAIISD-----------
OsRrp40     203 APSPSNVIVVSNAIIKSESLSGIGQR---------S--MVESLLERLS------------
SsRrp4      198 CPSRFSEEILIEAIRKIENESHIKGL---------TDRIKQFIEEKLGERNASSGETKTN
HsEXOSC2    207 PTPEHKEEEAGGF------IANLEPV---SL-------------------------ADR
ScRrp4      235 KTSQMDLARDTPSANNSSSIKSTGPTGAVSLNPSITRLEEESSWQIYSDENDPSISNNIR
consensus   301        l l   l   e                            l
```

```
HsEXOSC3        ------------------------------------------------------------
MmEXOSC3        ------------------------------------------------------------
DrRrp40         ------------------------------------------------------------
DmRrp40         ------------------------------------------------------------
CeRrp40         ------------------------------------------------------------
ScRrp40         ------------------------------------------------------------
SpRrp40         ------------------------------------------------------------
CnRrp40         ------------------------------------------------------------
AtRrp40         ------------------------------------------------------------
OsRrp40         ------------------------------------------------------------
SsRrp4      249 S-----------------------------------------------------------
HsEXOSC2    232 -------EVISRLRNCIISLVTQRMMLYDTSILYCYEASLPH-QIKDILKPEIMEEIVME
ScRrp4      295 QAICRYANVIKALAFCEIGITQQR-------IVSAYEASMVYSNVGELIEKNVMESIGSD
consensus   361

HsEXOSC3        ------------
MmEXOSC3        ------------
DrRrp40         ------------
DmRrp40         ------------
CeRrp40         ------------
ScRrp40         ------------
SpRrp40         ------------
CnRrp40         ------------
AtRrp40         ------------
OsRrp40         ------------
SsRrp4          ------------
HsEXOSC2    284 TRQ-RLLEQEG-
ScRrp4      348 ILTAEKMRGNGN
consensus   421
```

Figure S1 Protein sequence alignment of human EXOSC3, *S. cerevisiae* Rrp40, other EXOSC3/Rrp40 orthologs, human EXOSC2, *S. cerevisiae* Rrp4, and Archaeal Rrp4. Amino acids substituted in human EXOSC3 in PCH1b patients (WAN *et al.* 2012) and conserved in *S. cerevisiae* Rrp40 are highlighted in cyan. Amino acids substituted in human EXOSC2 in patients with novel syndrome (DI DONATO *et al.* 2016) and conserved in *S. cerevisiae* Rrp4 are highlighted in yellow. Identical residues (in red) and similar residues (in blue) that are conserved amongst orthologs are highlighted.

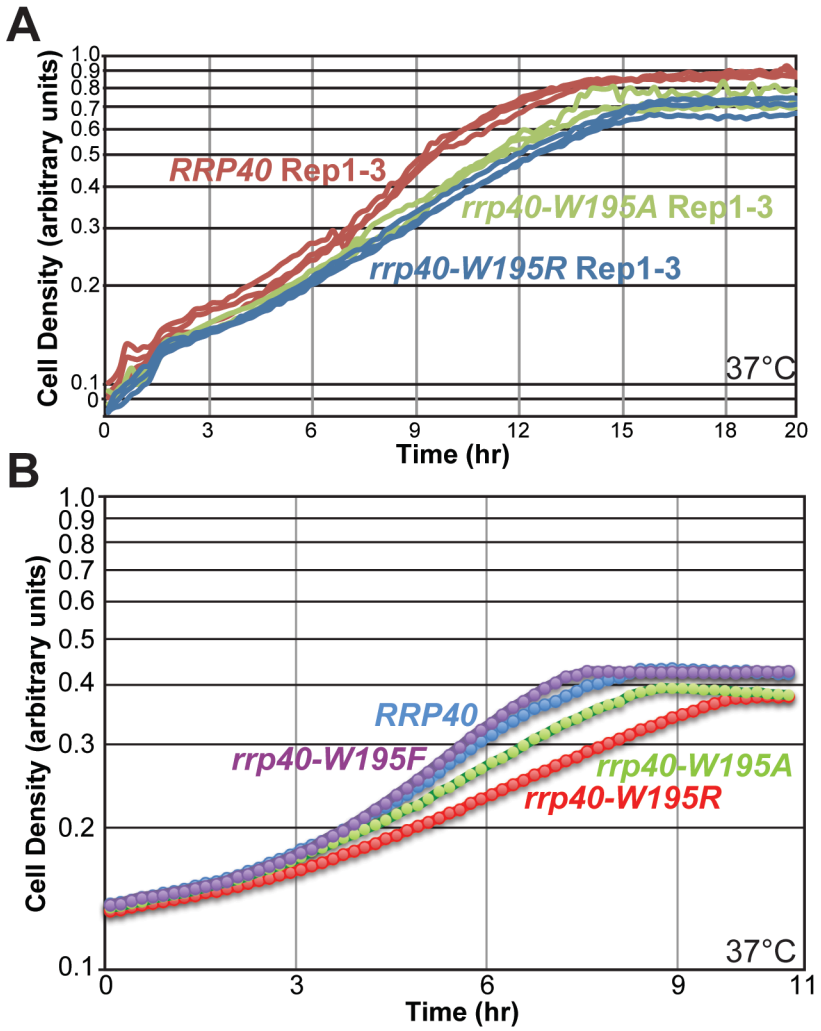

Figure S2 The *rrp40-W195R* mutant cells, but not *rrp40-W195F* cells, show slow growth at 37°C. *(A)* Triplicate biological replicates of the *rrp40-W195R* and *rrp40-W195A* mutant cells show slow growth at 37°C in liquid culture. *(B)* The *rrp40-W195F* mutant cells show growth similar to wild-type cells at 37°C in liquid culture. The *rrp40*Δ cells containing wild-type *RRP40* or mutant *rrp40* (*W195R; W195A; W195F)* plasmid were grown in liquid cultures at 37°C and optical density was measured over time.

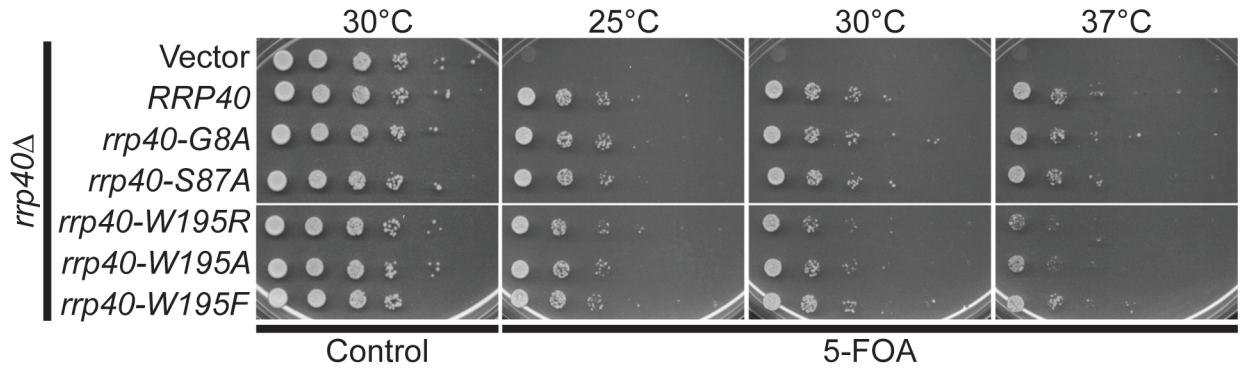

Figure S3 The *rrp40-W195R* and *rrp40-W195A* mutant cells show slow growth on 5-FOA plates at 30°C and 37°C in a plasmid shuffle assay. The *rrp40*Δ cells containing an *RRP40 URA3* maintenance plasmid and each mutant *rrp40* (*G8A; S87A; W195R; W195A; W195F)* were serially diluted and spotted on control or 5-fluoroorotic acid (5-FOA) plates and grown at indicated temperatures. Control plates select for cells that retain the *RRP40 URA3* maintenance plasmid and 5-FOA plates select for cells that have lost the *RRP40 URA3* maintenance plasmid.

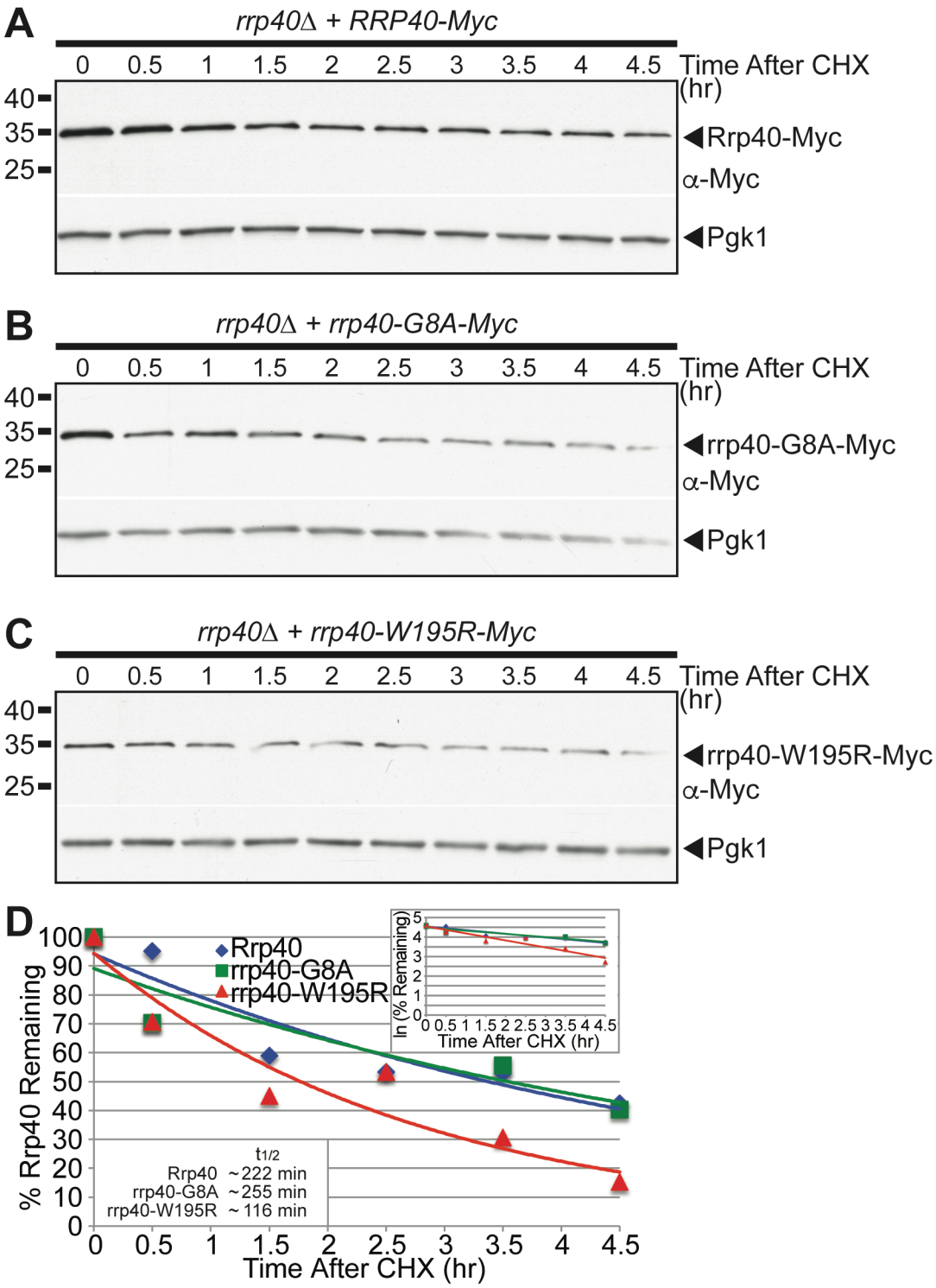

Figure S4 The rrp40-W195R variant, but not rrp40-G8A, is unstable in cells when expressed as only copy of Rrp40 at 30°C. *(A-C)* The protein levels of *(A)* wild-type Rrp40, *(B)* rrp40-G8A variant, and *(C)* rrp40-W195R variant expressed in *rrp40*Δ cells were assessed over time after cycloheximide treatment. *rrp40*Δ cells expressing Myc-tagged Rrp40 or rrp40 protein were treated with the translation inhibitor cycloheximide (CHX). Samples were collected over time (0-4.5 hours) and analyzed by immunoblotting with anti-Myc antibody to detect Myc-tagged Rrp40 and rrp40 protein (R/rrp40-Myc) and anti-Pgk1 antibody (Pgk1) to detect 3-phosphoglycerate kinase as a loading control. *(D)*

The immunoblots shown in *(A-C)* were quantitated to plot the percentage of Rrp40, rrp40-G8A, and rrp40-W195R protein remaining at each time point in *rrp40*Δ cells. The inset graph shows the natural logarithm (ln)-transformed percentages of Rrp40 and rrp40 protein at time points 0-4.5 hours fitted with linear least-squares fit lines to determine the decay rate constant (*k*) for each protein. The inset half-lives ($t_{1/2}$) of Rrp40 and rrp40 variants in *rrp40*Δ cells at 30°C were calculated from each decay rate constant using the equation $t_{1/2}=\ln(2)/k$ (BELLE *et al.* 2006). Further details on the measurement of the percentages of protein using protein band intensities and calculation of the protein half-lives are described in Materials and Methods. Quantitation is for specific experiment shown but is representative of multiple experiments.

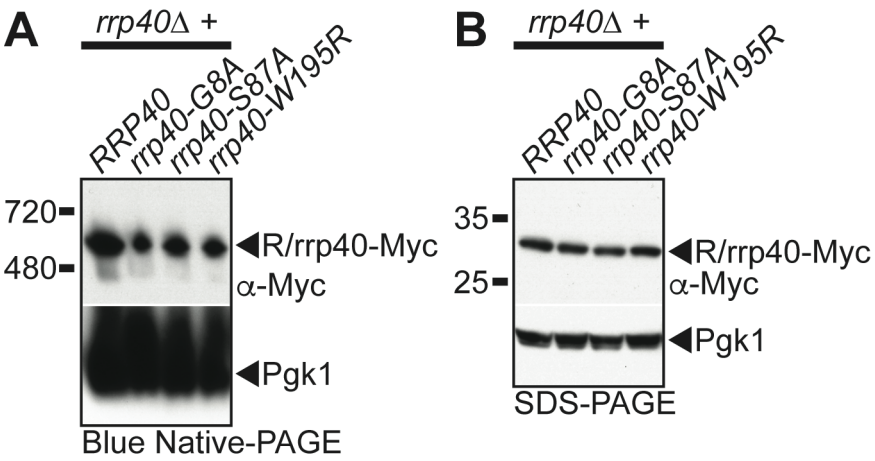

Figure S5 The rrp40-W195R variant associates efficiently with the RNA exosome complex when expressed as the only copy of Rrp40 in *S. cerevisiae* cells. *(A)* Similar to wild-type Rrp40, a reasonable amount of the rrp40-W195R variant in *rrp40*Δ cells migrates as a 600 kDa complex that is consistent with the size of the 11-subunit exosome (Liu *et al.* 2006) by native gel electrophoresis. The rrp40-G8A and rrp40-S87A variant also migrates as a 600 kDa complex. Lysates of *rrp40*Δ cells expressing Myc-tagged wild-type Rrp40 or variant rrp40 (G8A; S87A; W195R) were grown at 30°C and analyzed by blue native-PAGE and immunoblotting with anti-Myc antibody to detect Myc-tagged Rrp40 proteins (R/rrp40-Myc) and anti-Pgk1 antibody to detect 3-phosphoglycerate kinase (Pgk1) as a loading control. *(B)* In the same lysates analyzed by native PAGE in *(A)*, the amount of rrp40-W195R and other rrp40 variants in *rrp40*Δ cells is reasonably similar to wild-type cells analyzed by denaturing SDS-PAGE. Lysates were analyzed by immunoblotting anti-Myc antibody to detect Myc-tagged Rrp40 proteins (R/rrp40-Myc) and anti-Pgk1 antibody to detect 3-phosphoglycerate kinase (Pgk1) as a loading control.

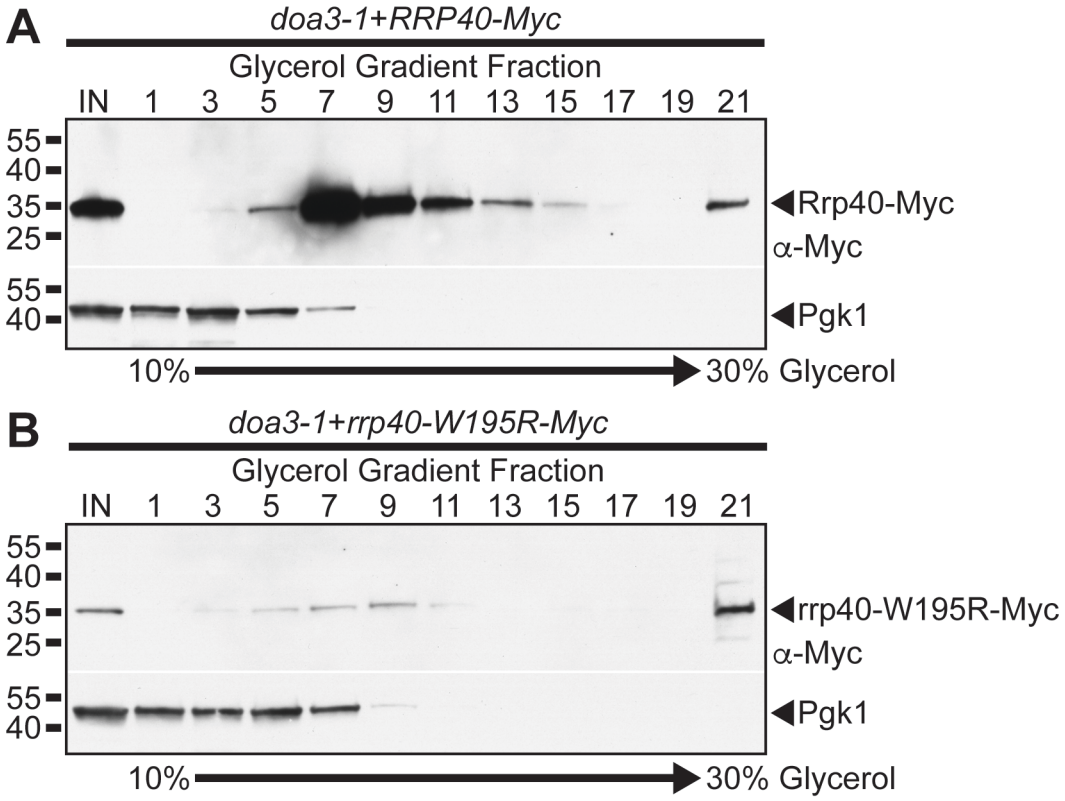

Figure S6 The rrp40-W195R variant associates less efficiently than wild-type Rrp40 with the RNA exosome complex in *S. cerevisiae* cells co-expressing wild-type Rrp40. *(A)* The majority of wild-type Rrp40 in *doa3-1* cells is present in fractions from the middle of the glycerol gradient (fraction 7-13) that most likely contain the exosome complex and much less Rrp40 is present in the heaviest fraction (fraction 21) by glycerol gradient fractionation. (B) Very little rrp40-W195R variant in *doa3-1* cells is present in fractions from the middle of the glycerol gradient (fraction 7-13) and the majority of rrp40-W195R is present in the heaviest fraction (fraction 21) by glycerol gradient fractionation. Lysates of *doa3-1* cells expressing Myc-tagged wild-type Rrp40 or rrp40-W195R variant grown at 37°C were analyzed by glycerol gradient fractionation and immunoblotting with anti-Myc antibody to detect Rrp40-Myc and rrp40-W195R-Myc and anti-Pgk1 antibody to detect 3-phosphoglycerate kinase (Pgk1), which is 44.7 kDa in size, as a gradient control.

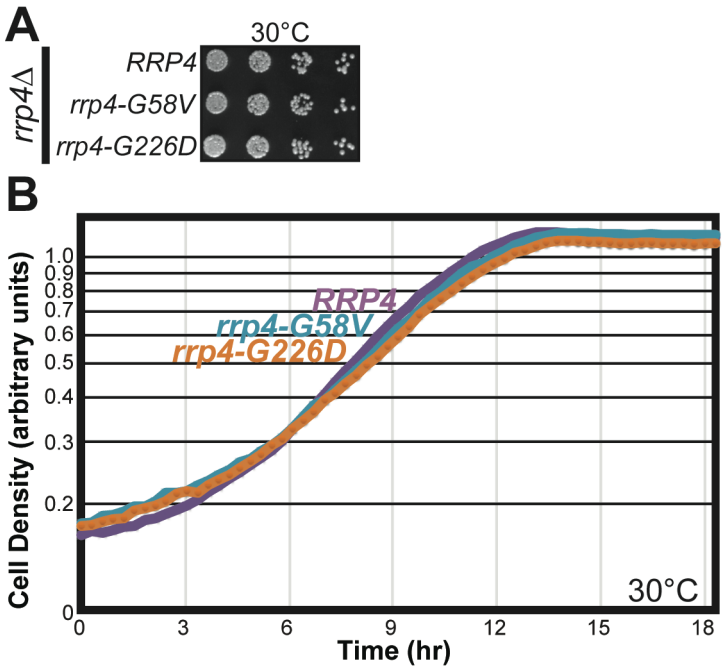

Figure S7 The *rrp4-G58V* and *rrp4-G226D* mutant cells, expressing rrp40 variants corresponding to disease-associated EXOSC2-G30V and EXOSC2-G198D variants identified in patients with a novel syndrome (Di Donato *et al.* 2016) (Figure S1), show growth similar to wild-type *RRP4* cells at 30°C. Growth of *rrp4*Δ cells containing wild-type *RRP4* or mutant *rrp4* (*G58V; G226D)* was analyzed by *(A)* serial dilution, spotting on minimal media plate, and growth at 30°C or growth in liquid cultures at 30°C and optical density measurements over time

Supporting Information Literature Cited

Belle, A., A. Tanay, L. Bitincka, R. Shamir and E. K. O'Shea, 2006 Quantification of protein half-lives in the budding yeast proteome. Proc Natl Acad Sci U S A 103**:** 13004-13009.

Chen, P., and M. Hochstrasser, 1996 Autocatalytic subunit processing couples active site formation in the 20S proteasome to completion of assembly. Cell 86**:** 961-972.

Di Donato, N., T. Neuhann, A. K. Kahlert, B. Klink, K. Hackmann *et al.*, 2016 Mutations in EXOSC2 are associated with a novel syndrome characterised by retinitis pigmentosa, progressive hearing loss, premature ageing, short stature, mild intellectual disability and distinctive gestalt. J Med Genet 53**:** 419-425.

Li, X., A. R. Kusmierczyk, P. Wong, A. Emili and M. Hochstrasser, 2007 beta-Subunit appendages promote 20S proteasome assembly by overcoming an Ump1-dependent checkpoint. EMBO J 26**:** 2339-2349.

Liu, Q., J. C. Greimann and C. D. Lima, 2006 Reconstitution, activities, and structure of the eukaryotic RNA exosome. Cell 127**:** 1223-1237.

Schaeffer, D., B. Tsanova, A. Barbas, F. P. Reis, E. G. Dastidar *et al.*, 2009 The exosome contains domains with specific endoribonuclease, exoribonuclease and cytoplasmic mRNA decay activities. Nat Struct Mol Biol 16**:** 56-62.

Sikorski, R. S., and P. Hieter, 1989 A system of shuttle vectors and yeast host strains designed for efficient manipulation of DNA in Saccharomyces cerevisiae. Genetics 122**:** 19-27.

van Hoof, A., P. A. Frischmeyer, H. C. Dietz and R. Parker, 2002 Exosome-mediated recognition and degradation of mRNAs lacking a termination codon. Science 295**:** 2262-2264.

van Hoof, A., R. R. Staples, R. E. Baker and R. Parker, 2000 Function of the ski4p (Csl4p) and Ski7p proteins in 3'-to-5' degradation of mRNA. Mol Cell Biol 20**:** 8230-8243.

Wan, J., M. Yourshaw, H. Mamsa, S. Rudnik-Schoneborn, M. P. Menezes *et al.*, 2012 Mutations in the RNA exosome component gene EXOSC3 cause pontocerebellar hypoplasia and spinal motor neuron degeneration. Nature genetics 44**:** 704-708.